# OPTIMIZATION OF WELL SETTINGS TO MAXIMIZE RESIDUALLY TRAPPED $CO_2$ IN GEOLOGIC CARBON SEQUESTRATION

**A REPORT SUBMITTED TO THE DEPARTMENT OF ENERGY RESOURCES ENGINEERING**

**OF STANFORD UNIVERSITY**

**IN PARTIAL FULFILLMENT OF THE REQUIREMENTS FOR THE DEGREE OF MASTER OF SCIENCE**

**By**
**Deepanshu Kumar**
**June, 2007**

I certify that I have read this report and that in my opinion it is fully adequate, in scope and in quality, as partial fulfillment of the degree of Master of Science in Petroleum Engineering.

_____

Prof. Louis Durlofsky
(Principal Advisor)

# Abstract

Geological sequestration is a potential technology for the long term storage of carbon dioxide ($CO_2$) emissions from stationary sources such as fossil fuel fired power plants. $CO_2$ injected into geological formations such as saline aquifers can be effectively immobilized by structural trapping, residual trapping, solution trapping and mineralization. In this work, previously developed optimization methods were modified and used for the optimization of $CO_2$ sequestration process. The optimization was based on the conjugate gradient (CG) method and used a commercial simulator as a "black box" for the calculation of numerical gradients. The main objective of the optimization was to determine optimal valve settings/injection rates for wells that maximize residual trapping of $CO_2$, so as to minimize the amount of $CO_2$ that is structurally trapped. This would mitigate the risk of leakage of the $CO_2$ to the atmosphere due to a loss in integrity of the formation cap rock.

First, 2-D simulations were carried out to study factors such as injection rates and aquifer properties that affect residual trapping and to verify that these factors were being captured by our models. Then, optimizations were carried out on a mildly heterogeneous, 2-D model for a variety of cases. It was shown that the optimization acted to increase the amount of residual trapping of $CO_2$ in the aquifer. When compared with an unoptimized two-well case, the optimization led to a decrease of 43% in the amount of structurally trapped $CO_2$. Optimization was also carried out on a 3-well case, which again produced significant improvements over the base case. Cases with high aquifer heterogeneity, a case with capillary pressure hysteresis and a case with a higher number of optimization steps were also studied to understand the effect of these factors on the optimized solution. The convergence of the optimization procedure to sub-optimal solutions was observed, however, so there is scope for improvements in algorithmic performance. There is also a need for enhanced computational efficiency, as the current algorithm is only suitable for cases with relatively few wells and well setting updates.

# Acknowledgments

I would like to express my sincere gratitude to my research and academic advisor Dr. Louis J. Durlofsky for his encouragement and guidance throughout the course of the M.S. program. I thank him for his advice and constant support which has made this work possible.

My thanks also go to Taku Ide and Yaqing Fan for valuable discussions, which provided me with a lot of helpful ideas. I am also grateful to Jerome Onwunalu for helping me with the code used in this work. I appreciate Dr. Burak Yeten and Inegbenose Aitokhuehi for their earlier work on the valve optimization module used in this study.

This work was prepared with the financial support of the industrial affiliates of the Stanford University Petroleum Research Institute for Advanced Wells (SUPRI-HW) and support from the Global Climate and Energy Project (GCEP). These contributions are gratefully acknowledged.

Special thanks are due to the entire staff (both teaching and administrative) and students of the Energy Resources Engineering department at Stanford, for creating a wonderful learning environment.

Finally, my love goes to my parents for their unwavering love and support at every step of my life.

# Contents

# List of Tables

# List of Figures

# Chapter 1

# 1. Introduction

It is now widely accepted that $CO_2$ emissions into the atmosphere are one of the major contributors to global warming. Three fourths of the global carbon emissions from human activities are due to the combustion of fossil fuels. In the US this figure is 82% (EIA data, May 2007). While a permanent solution to this problem would be to completely replace fossil fuels with alternative "clean" sources of energy, this can only be accomplished over a long period of time. It is however clear from climate studies that steps have to be taken in the very near future to begin to address the global warming threat. Since fossil fuels will continue to meet a large fraction of global energy demand for the foreseeable future, there is a need to develop energy efficient technologies and to mitigate the effects of those being currently used. $CO_2$ sequestration offers a promising approach to reduce substantially $CO_2$ emissions from the power and industrial sectors by capturing the $CO_2$ at the source and then storing it in geological formations. Considering the fact that these two sectors are responsible for approximately 60% of the global carbon emissions (EIA), $CO_2$ sequestration would appear to have real potential for alleviating the problem of global warming.

One of the major concerns associated with geological $CO_2$ sequestration is the potential leakage of $CO_2$ to the atmosphere. Such a leakage could occur due to a loss of integrity of the formation cap rock caused by overpressurization of the formation. It is therefore preferable that gas should not be trapped structurally (by structurally we mean against the cap rock) but via other mechanisms (e.g., as an immobile phase) to the extent possible. Assessment of this issue requires modeling techniques that include key physical effects and can simulate the sequestration process over long time periods. Computational

optimization techniques can then be applied to maximize the trapping of $CO_2$ as an immobile phase. These methods can provide us with optimum valve settings or injection rates for the wells, accounting for the geological heterogeneities and the fluid and formation properties. It is the goal of this report to begin exploring the application of optimization techniques for this purpose.

## 1.1. Literature Review

### *1.1.1. Mechanisms of $CO_2$ sequestration in Saline Aquifers*

In this study we consider $CO_2$ sequestration in saline aquifers. This is because saline aquifers appear to have the largest storage capacity for $CO_2$ (Gale, 2002). The sequestration process can be broadly broken into two phases. The first phase is the gas injection phase which typically lasts from 10-100 years depending on the size of project. During this phase, the $CO_2$ displaces the brine in the pore space. A portion of the $CO_2$ dissolves into the brine, though most of the injected gas remains in the gaseous phase. The brine with the dissolved $CO_2$ is denser than the original in situ brine and sinks towards the bottom. This form of $CO_2$ trapping is known as *solution trapping*.

In the second phase, there is no more $CO_2$ injection. The density difference between the $CO_2$ and the brine causes the $CO_2$ to migrate upwards to the top of the geologic structure. The cap rock stops the further upward movement of the gas, trapping it within the formation. This trapping phenomenon is called *structural trapping*. This type of trapping is not the preferable trapping mechanism for long-term $CO_2$ storage because the $CO_2$ is still mobile and any loss in the seal integrity of the cap rock could cause it to leak from the formation. There is another trapping mechanism which is important in this phase – *residual trapping*. As the $CO_2$ migrates upwards, it displaces the water at the leading edge while water replaces the $CO_2$ at the trailing edge of the $CO_2$ plume. We therefore have both imbibition and drainage occurring simultaneously. Due to hysteresis in the relative permeability curves and the residual gas saturation, a significant amount of $CO_2$ gets trapped in the pores as an immobile phase (Juanes *et al.*, 2006; Kumar *et al.*, 2005; Mo and Akervoll, 2005). This mechanism is discussed in detail later in this report. Since the

$CO_2$ trapped by this mechanism is immobile, this is a preferable trapping mechanism for storing $CO_2$ (as it cannot leak through the cap rock).

$CO_2$ also reacts with the minerals present in the brine and rocks. Various studies have been carried out to quantify the amount of $CO_2$ trapped by this mineralization mechanism. Nghiem *et al*. (2004) simulated the dissolution and chemical reactions of $CO_2$ with the formation minerals over large periods of time and demonstrated that these mechanisms do trap $CO_2$. Separate studies carried out by Izgec *et al*. (2005) and Pruess (2004) showed that while mineral trapping was less effective than solution trapping during the early periods of the sequestration process, the amount of $CO_2$ trapped by mineral trapping became comparable with solution trapped $CO_2$ at later periods of time.

These trapping mechanisms differ in terms of the amounts of $CO_2$ trapped and the associated time scales for these mechanisms. Kumar *et al*. (2005) performed a study of the $CO_2$ sequestration process, which included all of the major trapping mechanisms. They presented results indicating that the amount of $CO_2$ trapped by the residual trapping mechanism is much more significant than the $CO_2$ trapped by mineral or solution trapping mechanisms. Juanes *et al*. (2006) provided further evidence that the residual trapping mechanism does indeed result in trapping of $CO_2$ in large amounts as an immobile phase, and that this mechanism can be exploited to ensure a reliable $CO_2$ storage solution.

Works by Pruess *et al.* (2001), Kumar *et al.* (2005) and Mo *et al.* (2005) discussed the time scales associated with these mechanisms. Unlike residual and solution trapping, the mineral trapping mechanism occurs over much larger time frames. While $CO_2$ dissolution into the aqueous phase can be considered as an equilibrium process locally, it can be slow at the aquifer scale since it relies on the diffusion of $CO_2$ to regions not in contact with the $CO_2$ plume (Juanes *et al*., 2006). Mineral trapping, which is a function of reaction kinetics, would require tens of thousands of years to sequester substantial amounts of $CO_2$ (Pruess *et al*., 2001).

Taking these factors into consideration, it was decided to account just for residual and structural trapping in the simulations carried out for this study. The results presented in this work would therefore give a conservative estimation of trapped $CO_2$.

### *1.1.2. Optimization of Reservoir Performance*

The goal of this study is to use computational optimization to determine well settings that minimize structural trapping. This optimization can be performed for a reservoir model having a "smart well" (e.g., a well with downhole inflow control) or a model with two or more conventional wells.

The most general way to approach this problem is within a "closed-loop" reservoir management framework where the reservoir geology is unknown and the geological model is updated in time as new data are collected (Jansen *et al.*, 2005; Sarma *et al.*, 2006). The key components of this approach include efficient optimization and model updating (history-matching) algorithms and techniques for efficient uncertainty propagation (Jansen *et al*., 2005). For this study we do not use a "closed-loop" approach, but instead simplify the problem and consider "open-loop" reservoir management, in which well settings are optimized but the geology is assumed to be known. We take this approach because our intent for now is to study $CO_2$ injection strategies rather than model updating and uncertainty propagation.

As in previous studies (Jansen *et al*., 2005; Sarma *et al*., 2006; Yeten *et al*., 2002; Aitokhuehi and Durlofsky, 2005), the optimization here is carried out by calculating gradients of an objective function. The most computationally efficient approach would be to use an adjoint method to obtain the gradients (Jansen *et al*., 2005; Sarma *et al*., 2006). Adjoint approaches give all of the required gradients in one forward and one "backward" run of the simulator. This procedure however requires a linkage between the simulation model and the adjoint model at the level of source code. As a result, the implementation

of this approach requires extensive coding; the simulator cannot be treated as a "black box."

This study applies the numerical gradient approach implemented by Yeten (2003) and Yeten *et al.* (2002). The approach uses a commercial simulator (in this case ECLISPE $^{TM}$) as a black box for obtaining the objective function values. The gradients are then computed numerically (using a forward or backward difference method). Their approach entailed dividing the simulation period into equal optimization steps or time periods. Valve settings were then optimized in time for each of the optimization steps. They also investigated the effect of geological uncertainty and showed that it directly impacted the downhole settings. The use of numerical gradients is, however, much less efficient than the adjoint procedure. It is therefore viable only for cases with relatively few valves and limited updates of the valve settings. Otherwise, the procedure would require many function evaluations and would become too computationally demanding.

Within the context of $CO_2$ sequestration, Juanes *et al.* (2006) showed increased residual trapping with increased injection rates. Optimization algorithms would therefore be expected to exploit this effect along with the formation heterogeneities to minimize structural trapping.

## 1.2. Statement of Problem

As stated earlier, Yeten (2003) and Yeten *et al*. (2002) presented a procedure for optimizing smart well valve settings and Aitokhuehi (2005) and Aitokhuehi and Durlofsky (2005) expanded their work to combine valve optimization and history matching. The objective of this study is to use the optimization with known geology ("open-loop") to maximize the residual trapping of sequestered $CO_2$. Previous studies have shown that $CO_2$ injection rates and aquifer properties are important factors that affect residual trapping. The challenge is therefore to implement and test a procedure for the optimization of the injection rates, either for two or more conventional wells or

different segments of a smart well, for the purpose of maximization of residually trapped $CO_2$.

### *1.2.1. Solution Approach*

We approach the problem by first modifying the optimization code developed by Yeten (2003) so it can be applied for $CO_2$ sequestration problems. The objective function and the optimization algorithm were modified to minimize the structurally trapped $CO_2$ by optimizing the well settings for the injection phase of the project. The code was also changed so that it could be used with multiple wells. A number of cases were then considered, in order to assess the performance of the optimization procedure. The results show that optimization algorithm is effective in providing valve settings that reduce the amount of structurally trapped $CO_2$ relative to unoptimized base cases.

## 1.3. Report Outline

This report proceeds as follows:

**Chapter 2.** We present the factors that affect residual trapping of sequestered $CO_2$. Simulations are carried out on homogeneous and heterogeneous 2-D reservoir models to study the effects of hysteresis, injection rate and $k_v/k_h$ ratio.

**Chapter 3.** We discuss the solution method in greater detail and explain how well settings are optimized for this study. The conjugate gradient (CG) algorithm and its implementation are explained. The modifications introduced in the objective function and optimization algorithms are also discussed.

**Chapter 4.** Extensive simulation results for a variety of cases involving various well scenarios and degrees of heterogeneity are presented.

**Chapter 5.** We provide a summary and conclusions. Areas of future work are also suggested.

# Chapter 2

# 2. Geological $CO_2$ Sequestration

Several studies have examined the factors affecting the capillary trapping of sequestered $CO_2$. Kumar *et al*. (2005) assessed the sensitivity of the residual trapping to aquifer properties such as temperature, mean permeability, salinity, dip, $k_v/k_h$ ratio and the residual gas saturation (Kumar *et al*., 2005). Spiteri *et al*. (2005) and Juanes *et al*. (2006) investigated the effects of $CO_2$ injection rates and hysteresis on the overall performance of the sequestration project. Other studies have further validated the factors affecting the residual trapping (Bryant *et al*., 2006; Mo *et al*., 2005; Ide *et al*., 2007). Mo *et al.* (2005) suggested that increasing the viscous to gravity ratio results in more $CO_2$ trapping as residual gas. Bryant *et al.* (2006) stated that an appropriate choice of the $CO_2$ volume injected could also be an important factor to prevent the injected $CO_2$ from reaching the top of the aquifer where it might be subject to leakage.

Ide *et al*. (2007) investigated the interplay of viscous and gravity forces and capillary trapping of $CO_2$. They represented the effects of changes in injection rates and reservoir parameters in a single dimensionless gravity number, $N_{gv}$, a ratio of gravity to viscous forces (Zhou *et al.*, 1994). This number is defined as:

$$N_{gv} = \frac{k_v L \Delta\rho g}{Hu\mu}, \tag{2.1}$$

where $k_v$ is the vertical permeability, $L$ is the aquifer length, $\Delta\rho$ is the density difference between $CO_2$ and the in situ brine, $g$ is the acceleration of gravity, $H$ is the aquifer height, $u$ is the average flow velocity, and $\mu$ is the viscosity of brine. When $N_{gv}$ is large, gravity

forces dominate the flow and a thin gravity tongue forms at the top of the aquifer. When $N_{gv}$ is small, viscous forces are stronger, and a combination of the permeability distribution and viscous forces controls fluid movement.

Ide *et al*. (2007) concluded that $CO_2$ sequestration displacements with low gravity number trap significantly more $CO_2$ than displacements with strong gravitational forces relative to the viscous forces (high $N_{gv}$). This therefore means that a larger $u$ (higher injection rates), lower $k_v$ values (lower $k_v/k_h$ ratio) and low $\Delta\rho$ values (high reservoir pressure) would result in greater residual trapping of $CO_2$ (Eq. 2.1).

The principal petrophysical properties influencing residual trapping of $CO_2$ are relative permeability hysteresis and residual saturation of the non-wetting phase (Juanes *et al.*, 2006; Kumar *et al*., 2005; Mo and Akervoll, 2005). Both depend on the reservoir rock characteristics. Hysteresis is the phenomenon in which the relative permeabilities and capillary pressures depend on the saturation path and saturation history. It is the result of two processes:

1. Contact angle hysteresis: The surface of the pore walls contains minerals with different wetting characteristics towards the fluids in the pore structure. As a result, there is a difference between the advancing contact angle (of wetting phase displacing a non-wetting phase, i.e., imbibition) and the receding contact angle (of wetting phase being displaced by a non-wetting phase, i.e., drainage). The roughness of the rock surface also contributes towards this hysteresis.

2. Pore trapping: The pore size distribution and the ratio of the pore throat to pore body greatly impact the trapping of the non-wetting phase by the process of the snap-off of the non-wetting phase into small immobile "blobs."

We are studying the process of injection of $CO_2$ into an aquifer rock. The reservoir would therefore initially be fully saturated with brine. The rock grains of such a reservoir are

typically water-wet. The injected $CO_2$ would therefore be the non-wetting phase. During the gas injection period, the $CO_2$ phase invades the pore space and displaces the water phase. However, some amount of water remains in the $CO_2$ swept zone in the corners and crevices of the invaded pores and also in small pores where the $CO_2$ could not enter. It is important to note that there is not any trapping of $CO_2$ during this drainage process.

Once the $CO_2$ injection stops, the $CO_2$ phase continues to migrate upwards due to the density difference between $CO_2$ and brine. At the leading edge of the $CO_2$ plume, the $CO_2$ continues to displace water in a drainage-like process, while at the tail of the plume the voidage in the pore space created as a result of this $CO_2$ migration is filled by water, resulting in an imbibition type process. There are several mechanisms by which water can displace $CO_2$ during imbibition (Lenormand *et al.,* 1983). Of these, snap-off is the dominant mechanism in water-wet rocks (Al-Futaisi and Paztek, 2003; Valvatne and Blunt, 2004), which leads to the trapping of the $CO_2$ phase. These physical phenomena result in hysteresis.

The relative permeability hysteresis between drainage and imbibition for the non-wetting phase is illustrated in Figure 2.1. During the drainage process, the $CO_2$ saturation ($S_g$) increases and water saturation decreases and the relative permeability of the non-wetting phase follows the O-B-A curve. The water saturation at A is the irreducible saturation $S_{wi}$. If the drainage process is then followed by gravity segregation and the imbibing water phase replaces the gas phase, the relative permeability now follows the A-D curve. The water does not completely displace the gas and we have some $CO_2$ trapped in the pore space. This saturation ($S_{gtmax}$) corresponds to the $CO_2$ saturation at point D on the curve.

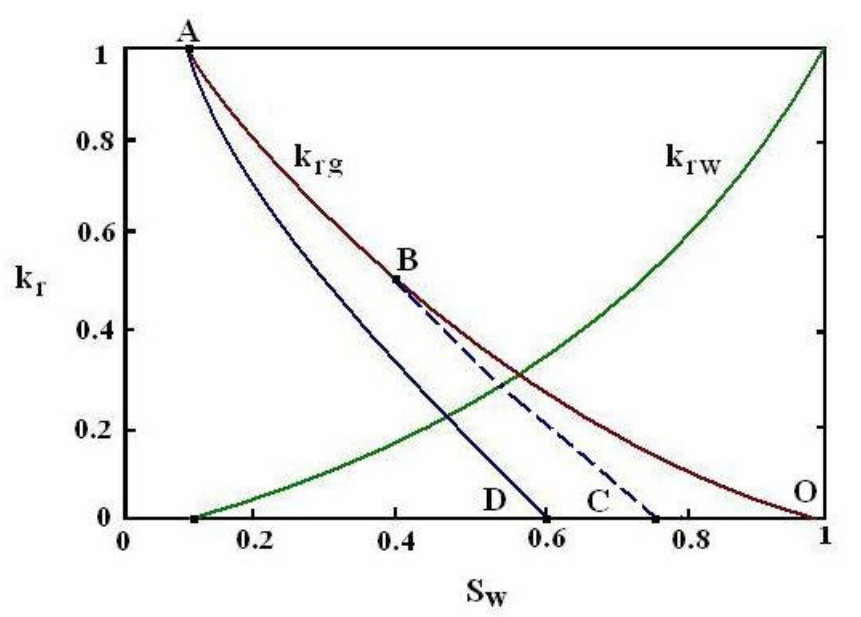


**Figure 2.1: Hysteresis effect for relative permeability**

The hysteresis in the residual gas saturation of the non-wetting phase also has an impact on the residual trapping of $CO_2$. Assume, for example, that during $CO_2$ injection, the gas saturation in a certain region proceeds only to point B. Now during the imbibition process, the residual (trapped) $CO_2$ saturation would not be $S_{gtmax}$ but some other saturation C ($S_{gt}$) shown in the figure. The imbibition curve would now be B-C (these curves are called scanning curves). To estimate the trapped gas saturation, we need to use a trapping model that relates the trapped gas saturation to the maximum gas saturation at the beginning of the imbibition process. The trapping model proposed by Land (1968) is commonly used for water-wet systems (Spiteri *et al*., 2005). In this model, the trapped gas saturation $S_{gt}$ is calculated as:

$$S_{gt} = \frac{S_{gi}}{1 + CS_{gi}} \tag{2.2}$$

where $S_{gi}$ is the initial gas saturation in the imbibition process and $C$ is the Land trapping coefficient. The Land trapping coefficient is computed from the bounding drainage and imbibition curves as follows:

$$C = \frac{1}{S_{gt\max}} - \frac{1}{S_{g\max}} \tag{2.3}$$

where $S_{gmax}$ and $S_{gtmax}$ are the maximum gas saturation and the maximum trapped gas saturation respectively. With the trapped gas saturation known, a relative permeability hysteresis model is used to calculate the relative permeabilities along the scanning curve. ECLIPSE has the option of using Carlson's hysteresis model, Killough's hysteresis model or Jargon's hysteresis model.

## 2.1. Numerical Simulations

Before proceeding with the optimization for $CO_2$ sequestration processes, we first study some of the factors which are expected to have an impact on the residual trapping to ensure that these factors are properly included in our models and that our results are consistent with the findings noted above. Simulations were performed for simple two-dimensional, vertical cross sections of the aquifers. $CO_2$ dissolution is not included in these simulations.

The data for the model is taken from Ide *et al.* (2007). The reservoir is assumed to be at 2500 m depth and fully saturated with brine. The aquifer is 800 m in length ($L_x$) and 40 m in height ($L_z$) and is represented by 400×40 grid blocks. The reservoir is 1 m thick ($L_y$) in the *y* direction. Fluid is injected through the bottom 10 m of the domain at the left end of the cross section and there is a vertical well at the right side of the reservoir producing at a fixed BHP of 250 bars (the wells are shown in Figure 2.2). For the base case, the $CO_2$ is injected at a rate of 1 reservoir $m^3$/day for a period of 1 year and the $k_v/k_h$ ratio is taken as 0.01. The injected volume of $CO_2$ was roughly 7% of the entire aquifer pore volume. The injection rates and the total amount of $CO_2$ injected were chosen such that the breakthrough of $CO_2$ did not occur in any of the sensitivity runs. In this work, we use the term gas as shorthand for "supercritical fluid." Two spatial distributions of permeability are studied – a homogeneous case and a heterogeneous case (Figure 2.2). The heterogeneous case was generated using S-GeMS (Remy, 2004), a geostatistical software

package developed by the SCRF group at Stanford University. The permeability realization was generated by Sequential Gaussian Simulation (sgsim). A spherical variogram model with $l_x/L_x$=0.25 and $l_z/L_z$=0.1 was specified, where $l_x$ and $l_z$ are the correlation lengths in the $x$ and $z$ directions respectively. The standard deviation of log permeability ($\sigma_{logk}$) is equal to 1 for the permeability field. The mean permeability value of the heterogeneous permeability field (164 md) was used for the homogeneous case.

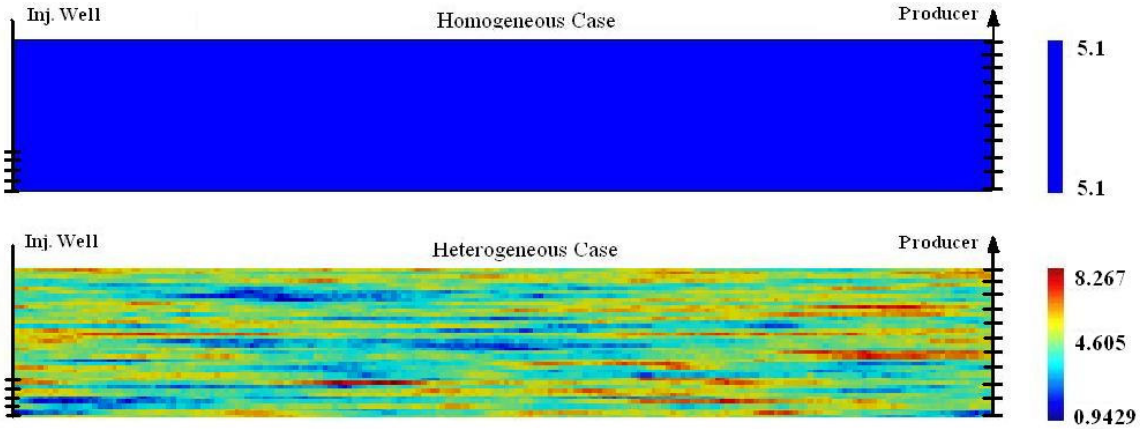


**Figure 2.2: Permeability fields (*log k*) and well locations**

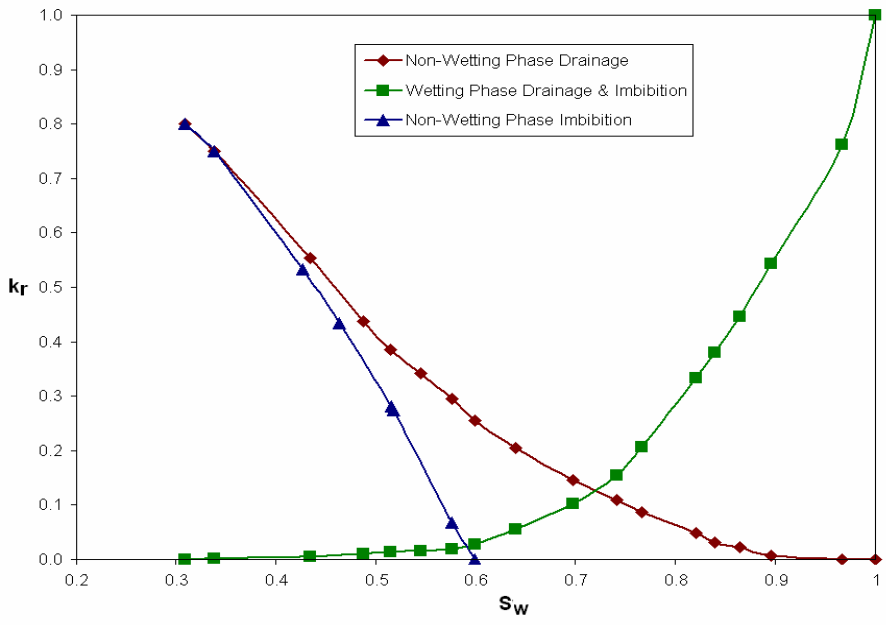


**Figure 2.3: Wetting and non-wetting phase relative permeability curves (adapted from Oak's data)**

Figure 2.3 shows the relative permeability curves used in this study. These curves have been adapted from the Oak data set (Oak *et al.,* 1990). Brine is assumed to be the wetting phase and $CO_2$ the non-wetting phase. The irreducible water saturation is 0.31, the residual gas saturation is 0.4 and the critical gas saturation is 0.033.

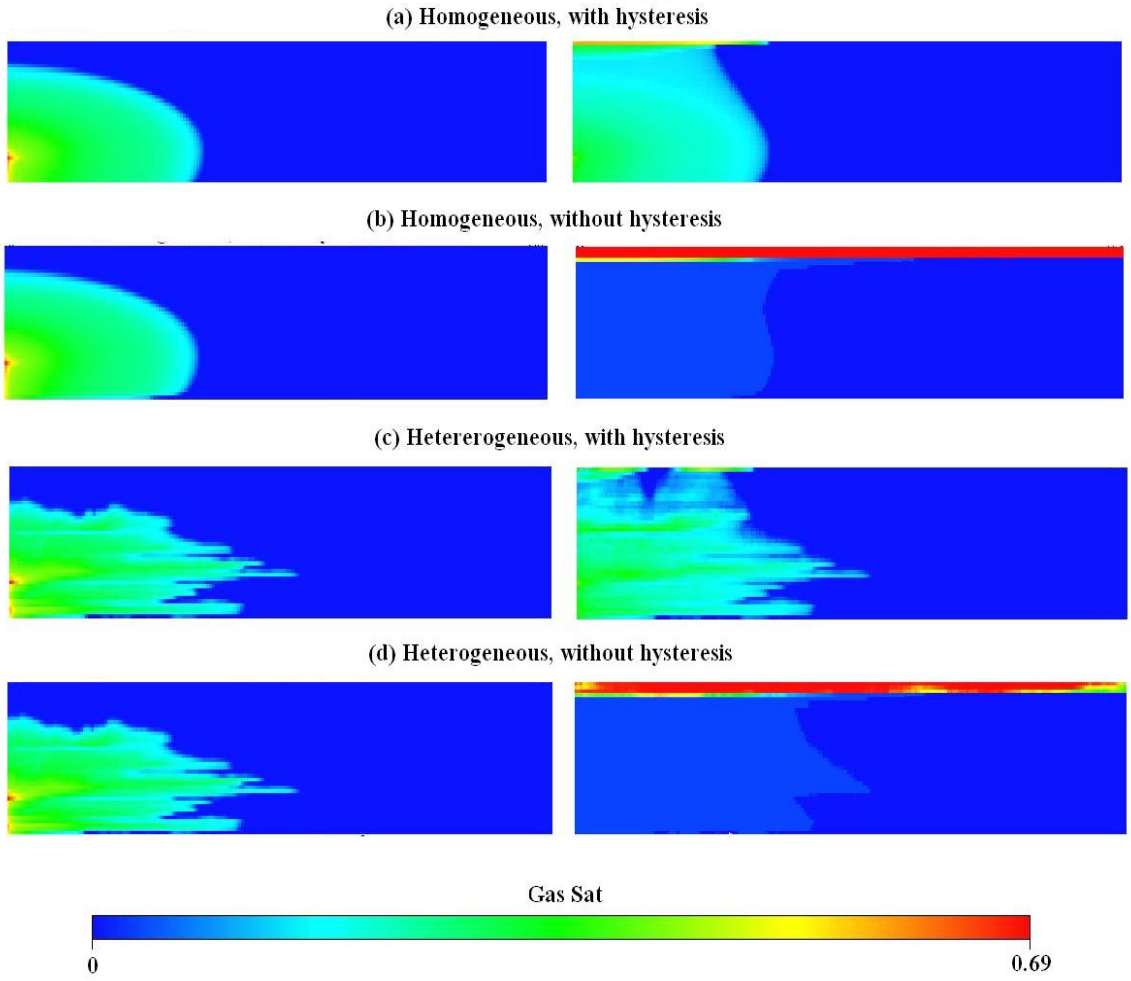


**Figure 2.4: Gas saturation in the reservoir after a 200 year shut-in period**

The impact of the hysteresis effect on residual trapping can be observed by simulating the $CO_2$ sequestration operation with and without hysteresis (Figure 2.4). Figures 2.4(a) and 2.4(c) show the results with hysteresis for the homogeneous and heterogeneous aquifers respectively, while Figures 2.4(b) and 2.4(d) show the results without hysteresis. These results clearly show that without hysteresis, given enough time most of the gas migrates to the top of the reservoir. Results such as these would lead one to conclude that there is

more risk associated with $CO_2$ sequestration than in actual fact. On the other hand, modeling the actual physics with the hysteresis model in the simulation leads to a significant amount of gas being trapped within the aquifer as an immobile phase.

The relative permeability functions shown in Figure 2.3 will be used for the remainder of the study. It is important to note however that varying the saturation end points would have a significant impact on the amount of gas trapped in the aquifer, as previous studies have indicated (Kumar *et al*., 2005; Mo and Akervoll, 2005).

## 2.2. Effect of Injection Rate

We now investigate the effect of injection rate on residual trapping. The same volume of $CO_2$ is injected over varying time periods. We first consider the homogeneous system. Case 2.1 is the base case with injection over one year. In Case 2.2 we inject over only 0.1 year, while in Case 2.3 we inject over 10 years.

The saturation distributions for the homogeneous case at different injection rates are shown in Figure 2.5. We can see that, for the low injection rate (Case 2.3), the amount of $CO_2$ reaching the top of the aquifer is greater. This is presumably because at lower injection rates the gravity forces are stronger than viscous forces and therefore affect the displacement of water by $CO_2$ at an earlier stage. For Case 2.3 the $CO_2$ gravitates to the top of the aquifer even before the injection is stopped. Since the $CO_2$ is trapped during imbibition, the fraction of $CO_2$ reaching the top during the injection period (drainage process) is not trapped and is therefore in a mobile phase. High injection rates (Case 2.2) increase the viscous forces (lower $N_{gv}$ value) and the gas front propagates further into the reservoir. As a result the injected gas contacts more of the reservoir. Once the injection stops, the $CO_2$ then migrates towards the top under gravity. Similar results were obtained for the heterogeneous case (Figure 2.6). The amount of residual trapping was greater for the case with high injection rate (Case 2.5) than for the base case (Case 2.4) or the case with a low injection rate (Case 2.6)

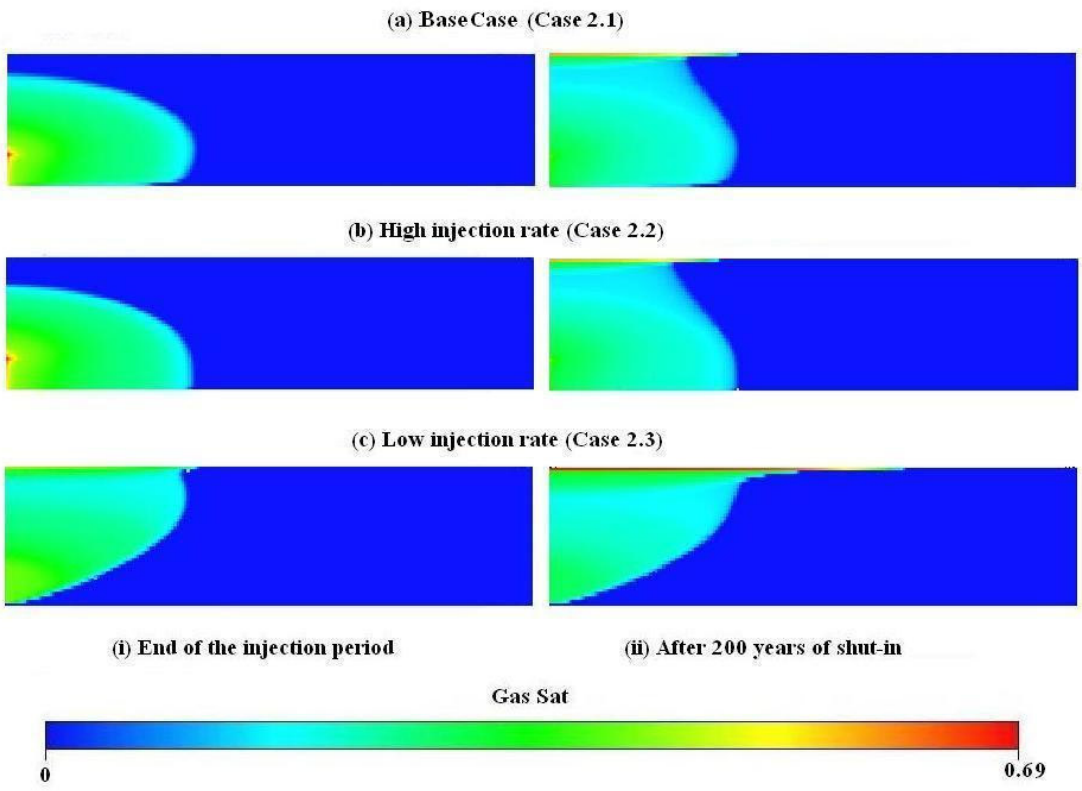


**Figure 2.5: Gas saturation distribution for different injection rates (homogeneous case)**

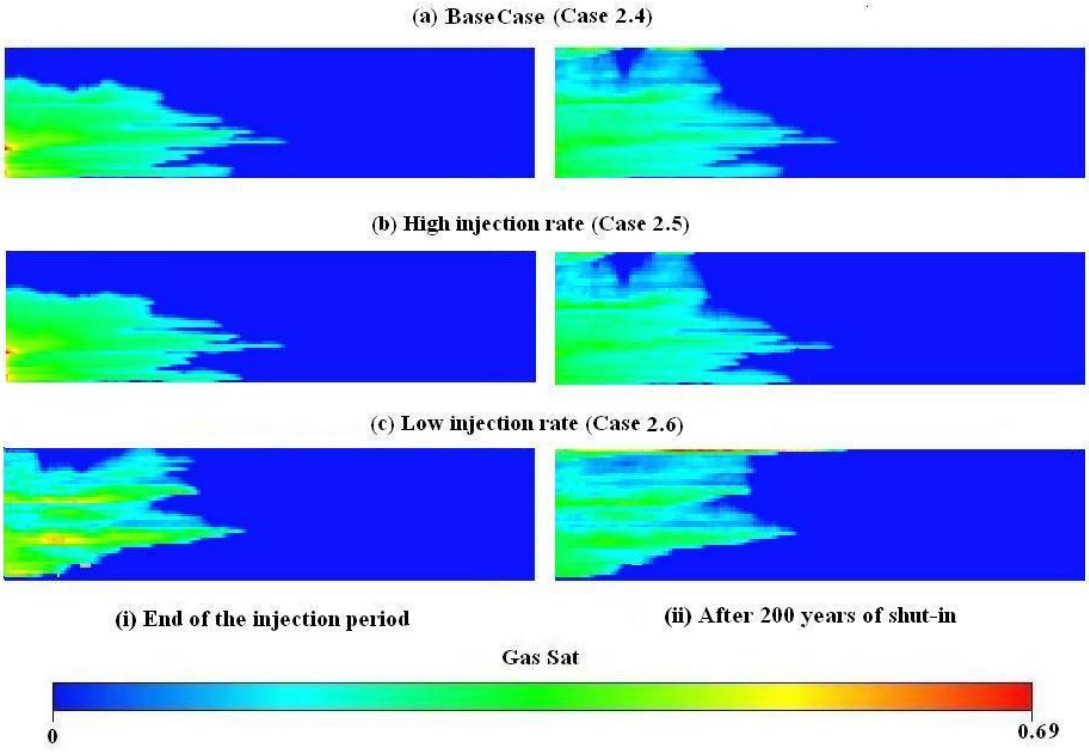


**Figure 2.6: Gas saturation distribution for different injection rates (heterogeneous case)**

## 2.3. Ratio of Vertical to Horizontal Permeability

Simulation runs for three different values of $k_v/k_h$ were carried out for the homogeneous case. The $k_v/k_h$ value for the base case (Case 2.7) was fixed at 0.01. The value was increased to 0.1 for Case 2.8 and reduced to 0.001 for Case 2.9. The value of $k_h$ was kept constant for all the three cases. Therefore, a high $k_v/k_h$ value translates to a high value of vertical permeability and a low $k_v/k_h$ value indicates that a low value of vertical permeability was used.

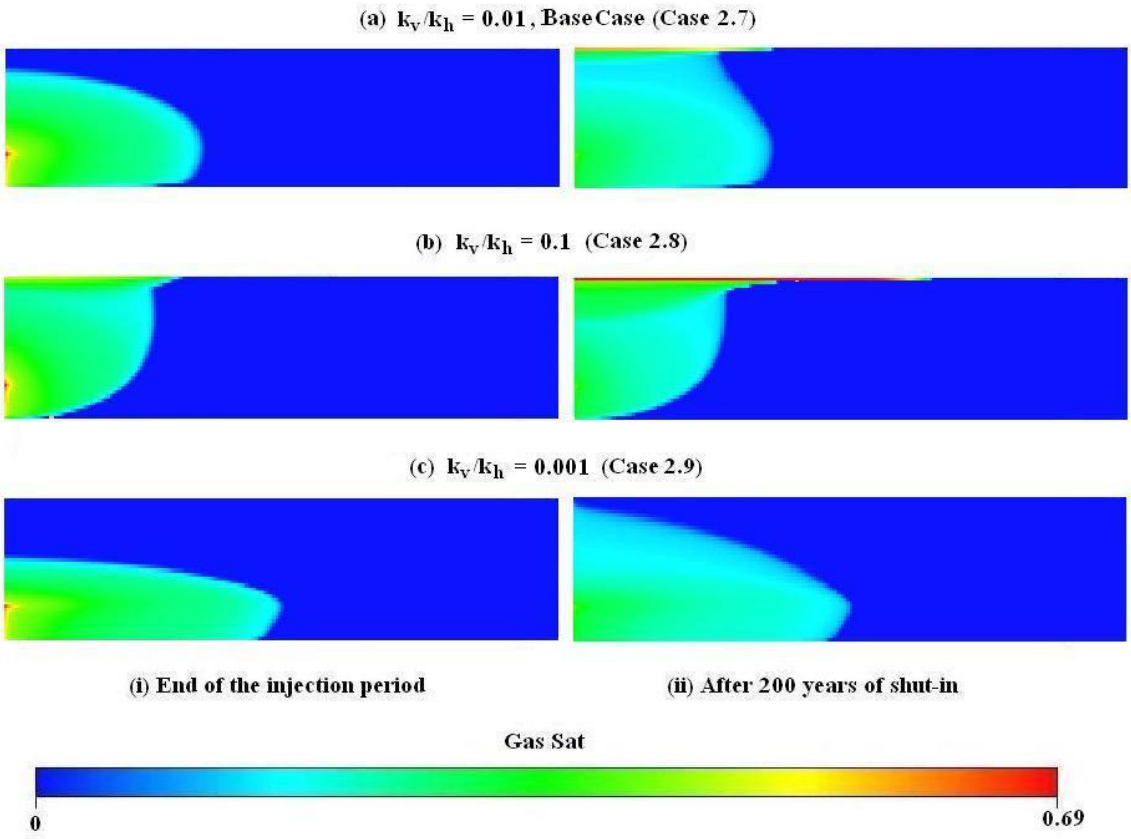


**Figure 2.7: Gas saturation distribution for different $k_v/k_h$ values (homogeneous case)**

Results for Case 2.7 ($k_v/k_h$ = 0.01) and Case 2.8 ($k_v/k_h$ = 0.1) clearly indicate that the higher the value of $k_v/k_h$ , the greater the amount of $CO_2$ that migrates to the top of the aquifer. In Case 2.9 ($k_v/k_h$=0.001), on the other hand, hardly any gas reaches the top of the aquifer. This is because the vertical migration is limited due to weak gravity forces, while the gas propagates further into the reservoir in the horizontal direction under viscous

forces. At larger $k_v$ values, we observe the formation of a gravity tongue with gas migrating to the top layer and most of the horizontal motion of the gas being restricted to the tongue. The gravity tongue continues to grow laterally at the top of the reservoir as vertical flow is restricted by the top boundary.

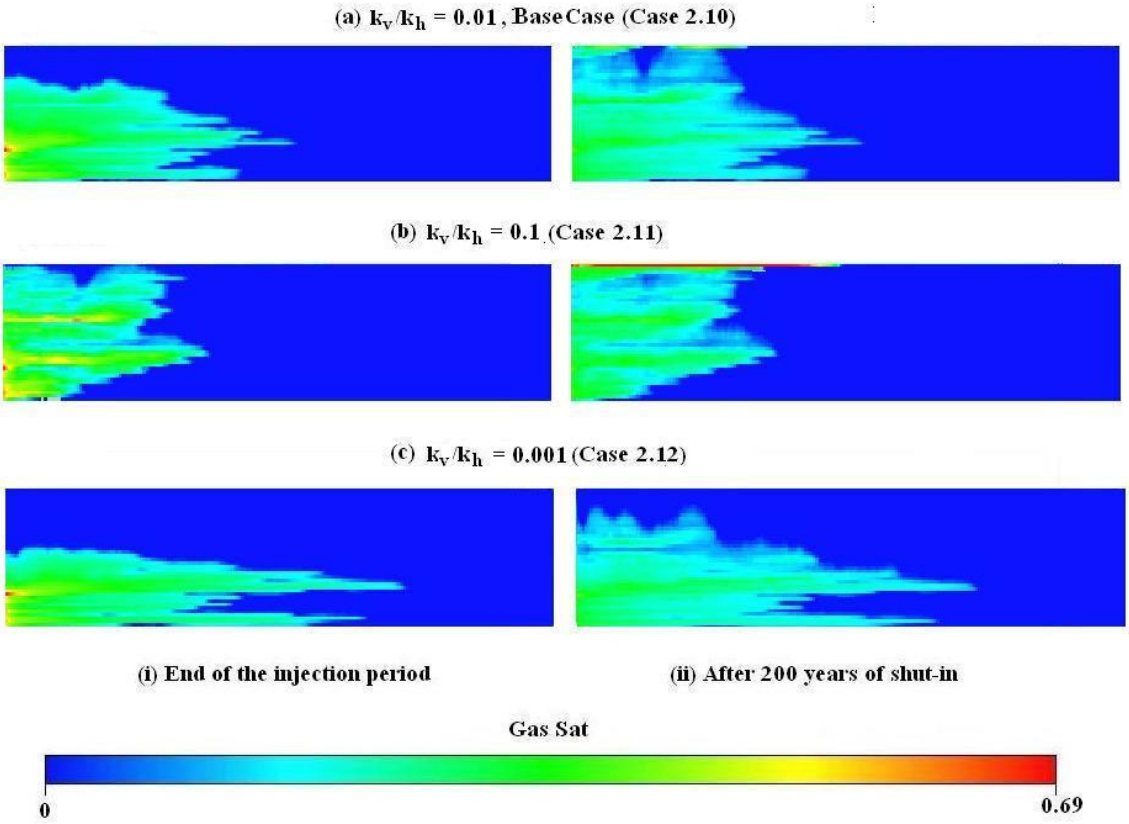


**Figure 2.8: Gas saturation distribution for different $k_v/k_h$ values (heterogeneous case)**

Figure 2.8 shows the results obtained for the heterogeneous case. We see results that are qualitatively similar to those for the homogeneous case, though high permeability layers lead to more spreading laterally. Again, low $k_v/k_h$ results in considerably lower gas saturations at the top of the reservoir.

Apart from the factors explored in this chapter, the dip of the formation also has a significant impact on the residual trapping of the gas. Kumar *et al.* (2005) showed that an increase in dip results in a greater fluid migration and hence more residual trapping.

Salinity of the brine and the reservoir temperature do not affect the residual trapping, but they play an important role in solution trapping.

# Chapter 3

# 3. Well Optimization

The well optimization used for this study utilizes the conjugate gradient (CG) procedure implemented earlier by Yeten (2003). The optimization routine exists completely outside the simulator though it calls the simulator for function evaluations. It can be used with multiple conventional wells or a smart well with two or more valves.

A smart well is a well with downhole instrumentation such as flow control valves, sensors etc. installed on the production tubing. The instrumentation allows for continuous in-situ monitoring of the downhole flow rates and pressures and periodic adjustments of the control valves. A smart well therefore provides greater flexibility in multilateral wells where production/injection for each lateral can be controlled independently. For a vertical well with multiple completions, the downhole instrumentation would again provide the ability to control the flow from or into each completion independently. ECLIPSE was the simulator used to model the smart wells.

## 3.1. Modeling of Wells

While ECLIPSE can be used to model multi-segment wells, in order to avoid complications arising out of cross-flow in between the completed segments, it was decided to model a smart well as a combination of two (or more) conventional wells (Figure 3.1). This representation would be expected to be sufficiently accurate in the case of concentric tubing completions.

As shown in the figure, the production tubing is represented as three segments: the completion segment, the segment representing the downhole choke and the segment representing the production tubing up to the wellhead. The fluid from the grid block enters the well through a nodal link and subsequently flows into the valve node and then the tubing segment.

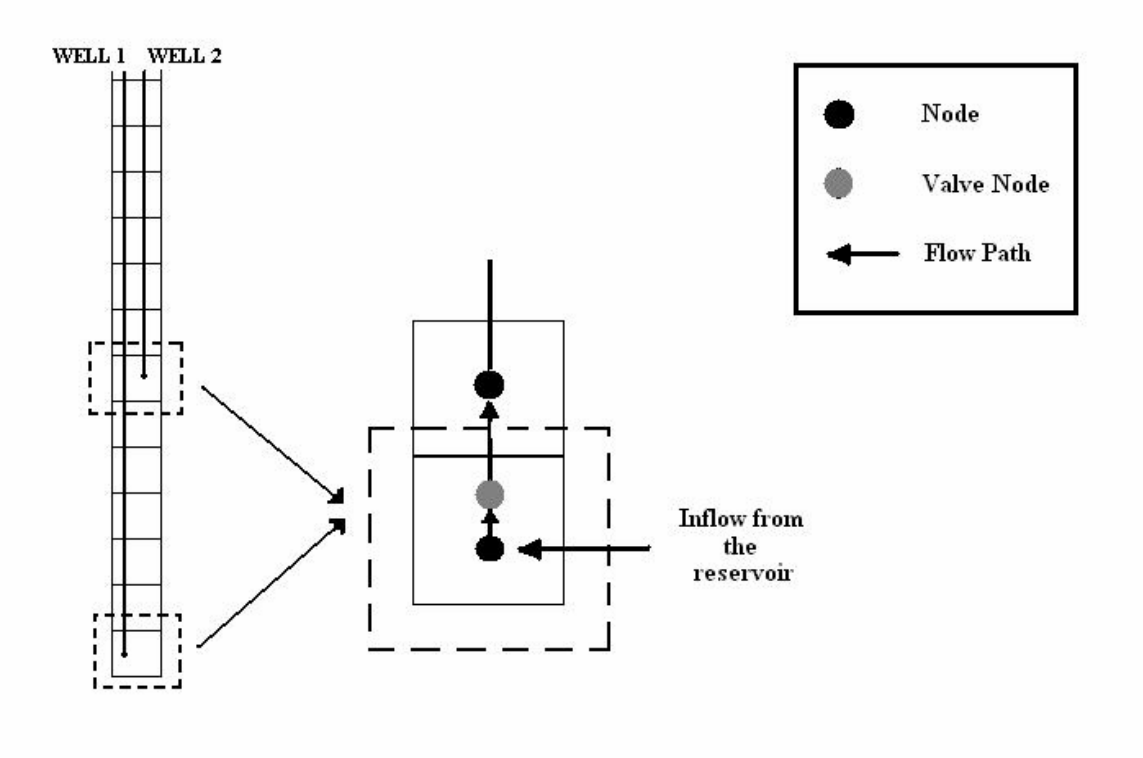


**Figure 3.1: Model of a well with two completion intervals**

## 3.2. Control Strategies

Wells can be operated under two kinds of control strategies, referred to as reactive and defensive control. Under reactive control, well settings are adjusted once problems occur (such as water breakthrough in an oil reservoir). This strategy generally involves trial and error to determine the ideal valve settings.

Under defensive control, optimum valve settings are determined prior to the start of production/injection using reservoir simulation so that future problems can be avoided or

mitigated. For oil production, the intent is to delay water and / or gas breakthrough and to accelerate production. Defensive control has been implemented using numerical gradients and a conjugate gradient method for "open-loop" optimization (Yeten, 2003; Yeten *et al*., 2002). Aitokhuehi and Durlofsky (2005) extended the procedure to cases where the geology of the formation is unknown (closed-loop reservoir management). In that work, valve settings that are optimal in an average sense over multiple geological realizations were determined.

The work presented in this report expands the application of the defensive control strategy to the problem of $CO_2$ sequestration in aquifers. The objective is therefore quite different from the previous applications of this strategy. Here, we use the strategy to take advantage of reservoir heterogeneities and injection rates to maximize the residual trapping of the injected $CO_2$.

## 3.3. Valve Control Optimization Module

We apply the nonlinear CG algorithm to determine the valve settings that maximize the residual trapping of injected $CO_2$. This is achieved by maximizing an appropriate objective function subject to production and injection constraints. This method utilizes the function gradient to determine the direction of change (increase or decrease) of the valve settings. The following sections describe the objective function and the CG implementation. This description follows closely that of Yeten (2003) and Aitokhuehi (2005).

### *3.3.1. Objective Function*

Since a primary concern with $CO_2$ sequestration is the leakage of the gas through the reservoir cap rock, our main goal is to maximize the trapping of gas within the reservoir in order to minimize the amount of gas reaching the top of the reservoir. The optimizations in this work therefore seek to minimize the gas saturation in the topmost layer of the reservoir. Hence if we maximize the brine saturation (or minimize gas saturation) in the top layer, we are essentially optimizing the trapping of gas in the

reservoir as an immobile phase (given that the simulation is run for sufficient time to ensure that equilibrium via gravity stabilization has been achieved).

For a given geological model, the objective function is stated as:

$$\underset{0 \le x_i \le 1}{\text{maximize}}\ F(x) = f \tag{3.1}$$

where $0 \le f \le 1$ is the average brine saturation of the topmost layer of the reservoir and $x_i$ is the scaled vector of valve settings ($x_i$ =0 corresponds to fully closed and $x_i$ = 1 to fully open).

### *3.3.2. Conjugate Gradient Algorithm*

The CG method is an algorithm for finding the nearest local minimum of a function of $n$ variables. The approach presupposes that the gradient of the function can be computed and uses conjugate directions instead of the local gradient for going "downhill." For any function approximated by a quadratic function, the gradient **g** is given as:

$$\mathbf{g(x) = -\,b + Hx} \tag{3.2}$$

where **H** is the Hessian matrix and **b** is an arbitrary vector. Hence the objective of the CG method is to find the **x** that gives $\mathbf{g(x)} \approx 0$. Since the gradient direction is opposite to the direction of descent, the residual, **r**, is set to the negative of the gradient. For our objective function in the previous section, this becomes:

$$\mathbf{r}^k = -\mathbf{F}'(\mathbf{x}^k) \tag{3.3}$$

where the superscript $k$ indicates the iteration level with $k$ = 0 referring to the initial guess. We define the vector **d** as the search direction, $\alpha$ is the step size in the search

direction and $\beta$ is the Gram-Schmidt constant. The outline of the CG algorithm used in this work is stated below (this description is taken directly from Yeten *et al*., 2002):

Given an initial guess, $\mathbf{x}^0$

Set $\mathbf{d}^0 = \mathbf{r}^0 = -\mathbf{F}'(\mathbf{x}^0)$

For $k = 0$ until $\mathbf{x}^k$ has desired accuracy

find $\alpha^k$ that minimizes $-F(\mathbf{x}^k + \alpha^k \mathbf{d}^k)$

$$\mathbf{x}^{k+1} = \mathbf{x}^k + \alpha^k \mathbf{d}^k \tag{3.4}$$

$$\mathbf{r}^{k+1} = -\mathbf{F}'(\mathbf{x}^{k+1})$$

$$\beta^{k+1} = \max\left\{\frac{(\mathbf{r}^{k+1})^T(\mathbf{r}^{k+1} - \mathbf{r}^k)}{(\mathbf{r}^k)^T \mathbf{r}^k}, 0\right\}$$

$$\mathbf{d}^{k+1} = \mathbf{r}^{k+1} + \beta^{k+1} \mathbf{d}^k$$

end

The algorithm is considered converged when

$$\left\| \mathbf{r}^k \right\| < \varepsilon \left\| \mathbf{r}^0 \right\| \tag{3.5}$$

with $\varepsilon$ here taken as 0.01. More details can be found in Yeten et al. (2002).

The gradient of the objective function is numerically computed using a forward finite difference approximation:

$$\mathbf{F}'(\mathbf{x}) = \nabla F(\mathbf{x}) = \frac{F(\mathbf{x} + h\mathbf{e}) - F(\mathbf{x})}{h} \tag{3.6}$$

where $\mathbf{e} = \{ e_i \}$ is a set of unit vectors and $h$ is the step size. Since for this study we use brine saturation as the objective function, the function value lies between 0 and 1. When the valve settings approach the upper limit (i.e., $x_i \rightarrow 1$), Eq. 3.6 is replaced with the backward difference approximation to avoid unphysical valve settings.

### *3.3.3. Implementation of the Algorithm*

The CG algorithm described in the previous section was implemented by Yeten *et al*. (2002) for optimization of smart well control. The algorithm is used here to minimize the gas saturation in the top layer of the reservoir. The simulations include an injection period followed by a stabilization period. The entire simulation period is divided into $n$ optimization steps at which valve settings can be changed. The valve settings for the first period ($t$=0 to $t=t_1$) are then optimized. For this optimization, the simulation is performed for the entire simulation period (injection and stabilization). For the next optimization period ($t=t_1$ to $t=t_2$), the optimization is performed from the time at the end of the previous optimization step to the end of the simulation period. The simulation is therefore restarted from the end of the previous optimized step (see Figure 3.2). This is repeated for the subsequent optimization steps. At each optimization step, we optimize over the entire simulation period and not just over that particular simulation period to avoid a situation where the "optimal" valve settings are optimal only for that period, but have detrimental effects in the long run. This approach therefore ensures that the optimized valve settings determined for earlier time steps will not affect the optimization at later times in a negative way.

The optimization procedure is specified as follows (Yeten *et al*., 2002):

1. The simulation period is divided into $n$ time periods at which the settings will be updated to optimize the objective function.

2. For each period $i$, the valve settings are optimized such that they minimize the objective function for the remaining simulation period.

3. Restart the simulation from the end of the previous period.

4. Repeat steps 2 and 3 until the entire simulation period is covered.

The overall process is depicted in Figure 3.2. In this figure each color represents an optimized valve setting for the specific time period. The circles on this figure represent the restart points which coincide with the end of an optimization period.

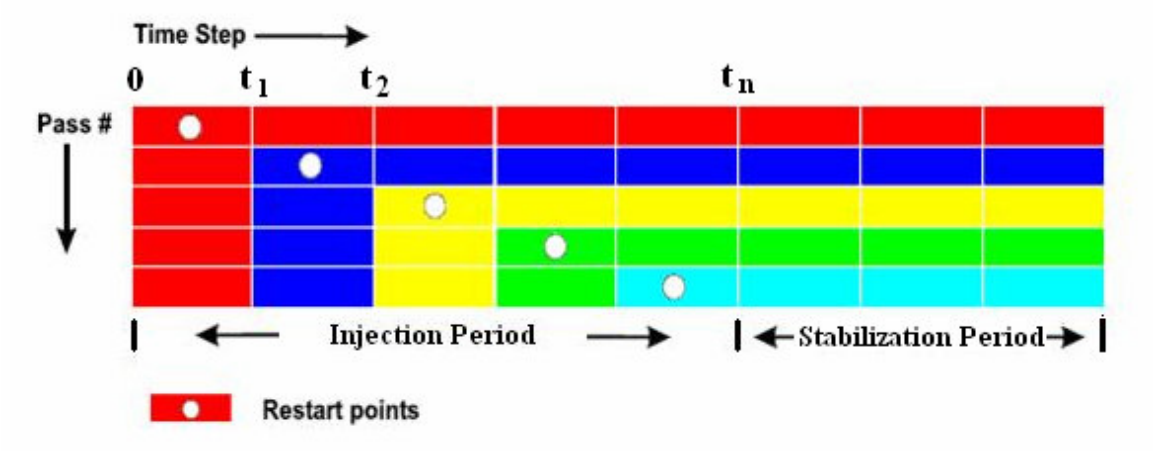


**Figure 3.2: Technique for the optimization of valve settings in time**

The previous algorithm was modified in this work to make it applicable for the $CO_2$ sequestration process. Since migration of $CO_2$ occurs over a long period of time, the simulation is run for another two hundred years after the end of the injection period. The valve settings are however determined only for the injection period as indicated on Figure 3.2.

We note finally that the CG method will in general converge to a minimum that depends on the initial starting point and the solution surface. The sensitivity of the optimal well settings to the initial guess can be investigated by running the method for different initial settings, as discussed later in Chapter 4.

# Chapter 4

# 4. Results and Discussion

We now apply the optimization procedure described in Chapter 3 to model problems. We first describe the numerical models used in the simulations and then present optimization results for a variety of cases.

## 4.1. Simulation Model

For the first set of cases (Case 4.1 to Case 4.9), simulations were performed for a mildly heterogeneous two-dimensional, vertical cross section of an aquifer. The model parameters used in the simulations are listed in Table 4-1. A total of 16,000 grid blocks was used in the simulations. Capillary pressure and gas solubility were not included in these simulations (capillary pressure is included in later simulations). A grid block aspect ratio of 2:1:1 (length/height/thickness) was used.

**Table 4-1: Simulation model parameters for Cases 4.1 to 4.9**

| Parameter | Values |
|---|---|
| Size | 40,000 ×50×2000 $ft^3$ |
| Tops | 1000 ft |
| Porosity | 0.135 |
| Pressure | 2000 psi |
| Temperature | 104 $^oF$ |
| Grid | 400 ×1×40 |
| Avg. permeability | 1100 mD |

The permeability field was generated using S-GeMS (Remy, 2007). Sequential Gaussian Simulation (sgsim) was used to obtain a permeability realization. A spherical variogram model with $l_x/L_x$=0.5 and $l_z/L_z$=0.1 was specified, where $l_x$ and $l_z$ are the correlation lengths in the $x$ and $z$ directions respectively. The standard deviation of the log of permeability ($\sigma_{logk}$) for this permeability field is equal to 0.3 and the $k_v/k_h$ ratio was taken to be 0.1 No hard data were used for permeability generation. The permeability realization used for the flow simulations is shown in Figure 4.1.

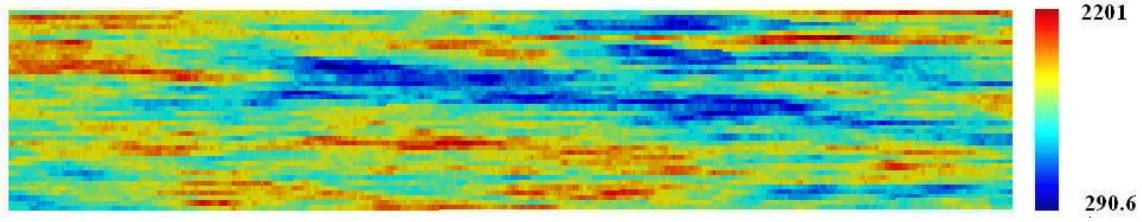


**Figure 4.1: Permeability field**

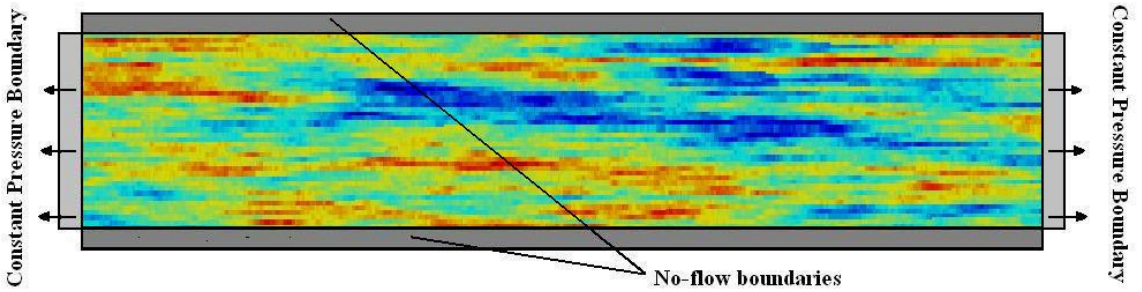


**Figure 4.2: Boundary conditions**

Appropriate boundary conditions (no-flow and fixed pressure) were applied to the simulation grid. The lateral boundaries were modeled as constant pressure boundaries to represent the continuity of the aquifer. These boundaries were represented by high pore volume cells in the simulations. The top and the bottom boundaries of the simulation were modeled as no-flow boundaries (Figure 4.2).

For convenience, the simulation grid was conceptually divided into two regions. The first region was composed of all the grid blocks in the topmost layer. This was done so that the average brine saturation of the region could be directly used as the objective function for the optimization process. However since the grid blocks at the boundaries with high pore

volumes would have skewed the average brine saturation values towards the higher end, the lateral boundaries for the topmost layer did not include high pore volume cells. The rest of the layers were allocated to region 2.

The injection rate for the study was selected as follows. A 1000 MW bituminous pulverized coal plant with 85% capacity factor and 90% efficient capture produces a $CO_2$ stream mass of approximately 6.24 million tons/yr (Friedmann and Herzog, 2006). If injected at a depth of 1000 ft (the depth of the simulation model under study), the volume rate of supercritical $CO_2$ would be around 200,000 bbl/d. Considering that the greatest injection rate for any well in the world is 40,000 bbl/d and that the typical rates in the US are less than 3000 bbl/d (Friedmann and Herzog, 2006), we would need tens of vertical wells or a number of high-reach horizontal wells for sequestering the $CO_2$ emissions from a coal plant. Since we are injecting in a 2-D vertical section of a larger aquifer, we used an injection rate of around 6000 mcf/d (using FVF=0.0034 $rft^3/ft^3$, this rate corresponds to $6\times10^6$ scf/d = 3634 reservoir bbl/d), which lies within the limits of practical injection rates. The $CO_2$ was injected over a period of 10 years (the typical lifetime of a large coal plant is about 50 years). The rate and total volume of the $CO_2$ injected were also chosen such that the $CO_2$ does not reach the reservoir boundaries (assumed to be spill points) over the duration of the simulations. The PVI calculations are given below:

**Reservoir Pore Volume** = Bulk rock volume × φ
= 40000 ft × 50 ft × 2000 ft × 0.135
= 540,000 mcf (reservoir conditions)

**Formation Volume Factor (FVF)** = 0.0034 $rft^3/ft^3$ (from Ennis King, 2006, at reservoir conditions)

**Total volume injected** = 6000 mcf/d × 365 days × 10 yrs
= 21,900,000 mcf (standard conditions)
= 74,460 mcf (reservoir conditions)

**PVI** = 74,460 / 540,000 × 100 = ~ 13.8 %

## 4.2. Simulation Results

The properties of $CO_2$ and brine were estimated with the correlation of Ennis-King (2006). Pure supercritical $CO_2$ was injected at a constant field rate of 6000 mcf/d (3634 reservoir bbl/d) for 10 years, followed by 200 years of well shut-in, during which the $CO_2$ migrates towards the top of the reservoir due to the density contrast (again, the term "gas" or "$CO_2$" in this chapter is shorthand for "supercritical fluid"). During the sequestration process, part of the $CO_2$ dissolves into the brine and part remains in the gaseous phase. In this study we do not model the dissolution of $CO_2$ into brine as noted earlier.

### *4.2.1. Single-Well Case*

For this case, we run the optimization for the simulation model with a single well at the center of the grid. The well is a multi-segment well completed in two separate intervals. As explained previously in Section 3.1, for convenience we model this well as two conventional wells. The first well is completed in the grid block (200, 1, 40) and the second in the grid block (200, 1, 28). Both these grid blocks lie in high permeability regions of the reservoir.

For the base case (Case 4.1), we inject the same volumes of $CO_2$ through the two intervals. The gas saturations at the end of injection period and at the end of the shut-in period are shown in Figure 4.3 and Figure 4.4. From these figures we clearly see that a significant amount of $CO_2$ reaches the top of the reservoir even before the injection is stopped. This is because the $CO_2$ injected from the upper interval travels to the top in less time as it has to rise through a shorter distance compared to gas injected from the bottom interval. Once this $CO_2$ reaches the top, it is no longer subjected to residual trapping.

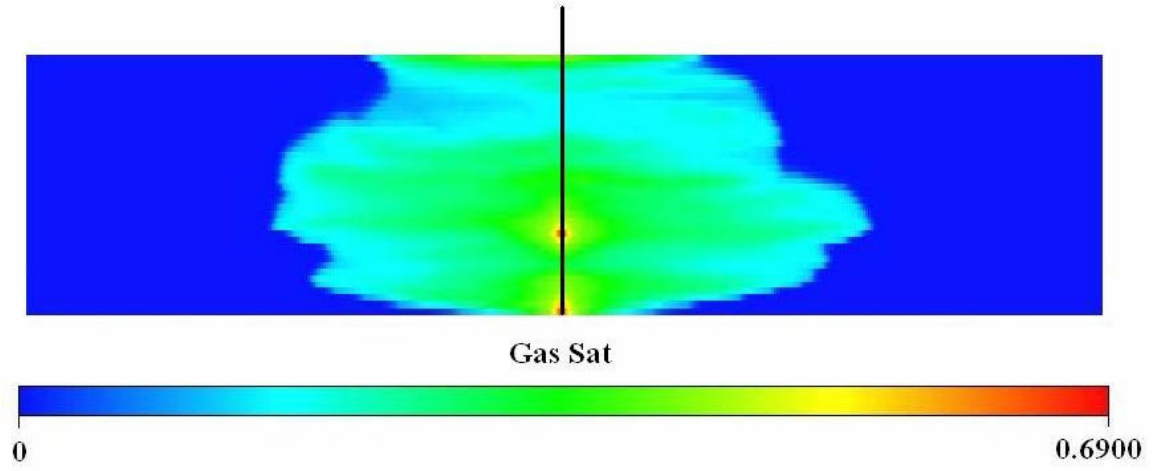


**Figure 4.3: Gas saturation distribution at the end of injection period (Case 4.1: base case)**

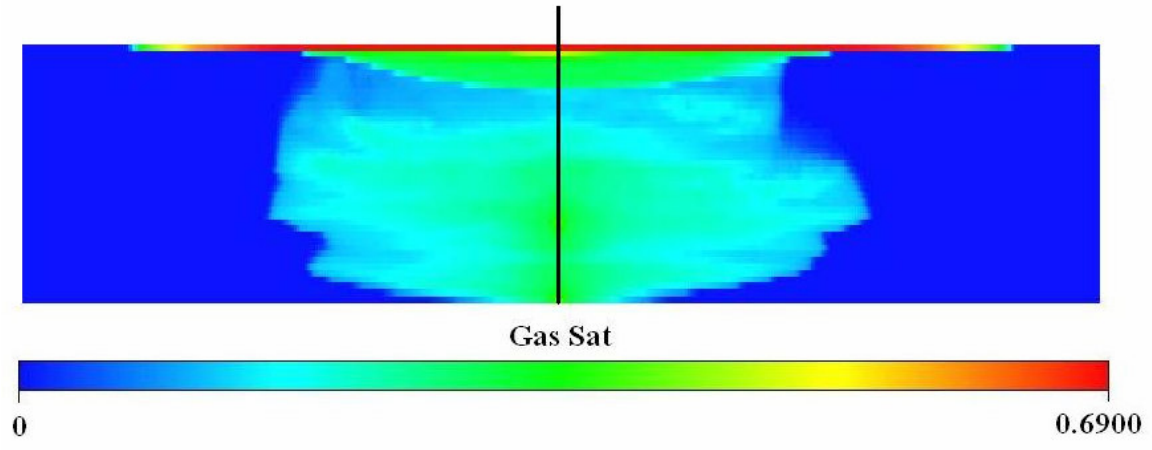


**Figure 4.4: Gas saturation distribution at the end of shut-in period (Case 4.1: base case)**

We then carry out the optimization to determine the injection rates into the two intervals that would maximize the residual trapping of $CO_2$. The saturation distributions at the end of the injection period and the end of shut-in period are shown in Figures 4.5 and 4.6. The optimized valve settings and the corresponding injection rates are presented in Table 4-2.

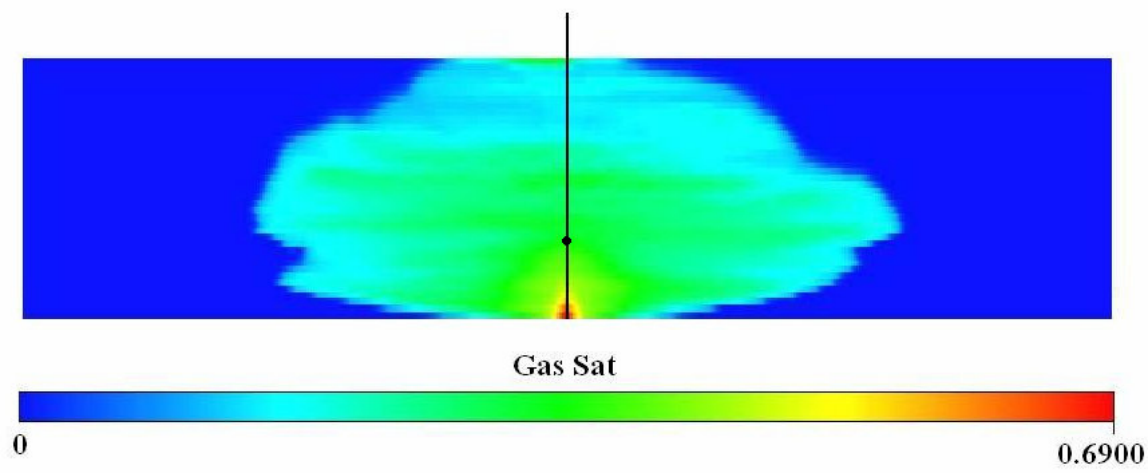


**Figure 4.5: Gas saturation distribution at the end of injection period (Case 4.2: optimized case)**

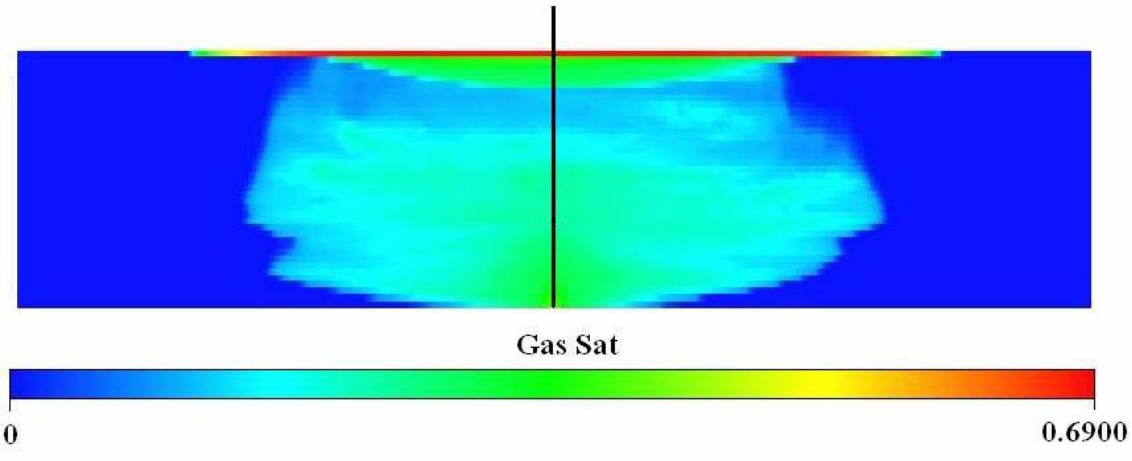


**Figure 4.6: Gas saturation distribution at the end of shut-in period (Case 4.2: optimized case)**

From Table 4-2 we can see that valve #2 was shut off for the entire duration of the simulation. The optimized solution for this case was therefore to not inject from the upper interval, but to inject all the $CO_2$ from the bottom interval. Optimizations carried out for the same case, but with different depths of the top completion interval, produced the same solution - that all of the gas is injected from the bottommost interval. Since all the gas is injected from the bottom completion, the amount of gas reaching the top of the reservoir by the end of injection period is somewhat less than in the base case (compare Figures 4.3 and 4.5). As the gas in the rest of the aquifer moves upwards under gravity, a greater

amount gets trapped as an immobile phase, resulting in lower gas saturation in the top layer of the aquifer (compare Figures 4.4 and 4.6).

**Table 4-2: Valve Settings for Case 4.2 (optimized 1-well case)**

| Time (up to) | Valve #1 (Lower Completion) | Valve #2 (Upper Completion) |
|---|---|---|
| 730 days | Fully Open | Fully Closed |
| 1460 days | Fully Open | Fully Closed |
| 2190 days | Fully Open | Fully Closed |
| 2920 days | Fully Open | Fully Closed |
| 3650 days | Fully Open | Fully Closed |

The gas saturation in the top layer of the aquifer in Case 4.1 (base case) was **0.5257** while for the Case 4.2 (optimized case), it was **0.4421.** The optimization therefore results in a **decrease of 16%** in the amount of gas that is structurally trapped.

These results underscore the need to complete the wells as far away from the top of the reservoir as possible. This finding is rather intuitive, though it is reassuring that the optimization produced the expected result in this case. Similar results were obtained by Kumar *et al.* (2005), who recommended completing the well in the bottom half of the reservoir. Janssen *et al.* (2005) too concluded that injecting far from the top of the reservoir was an important step towards optimizing a $CO_2$ injection strategy.

### *4.2.2. Two-Well Case*

For this case, we have two wells in the reservoir instead of a single well. These wells are located at (150, 1, 40) and (250, 1, 40). The wells were placed such that there was minimal well to well interaction and a very small boundary effect. Optimization was then carried out to determine the optimal injection rates for the individual wells.

For the base case (Case 4.3), the same amount of $CO_2$ was injected from the two wells. The gas saturation distributions at the end of the injection and shut-in periods for this case are shown in Figure 4.7 and Figure 4.8.

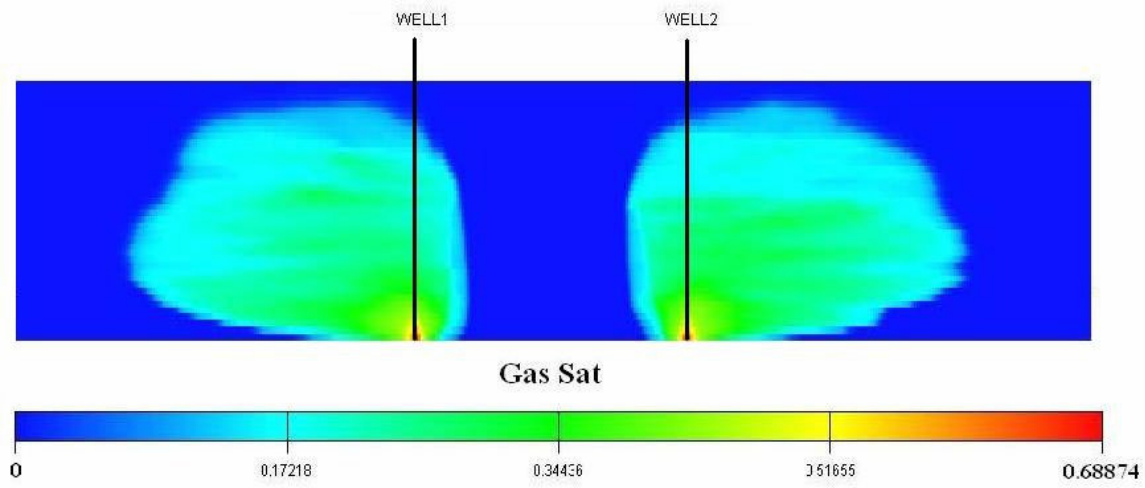


**Figure 4.7: Gas saturation distribution at the end of injection period (Case 4.3: base case)**

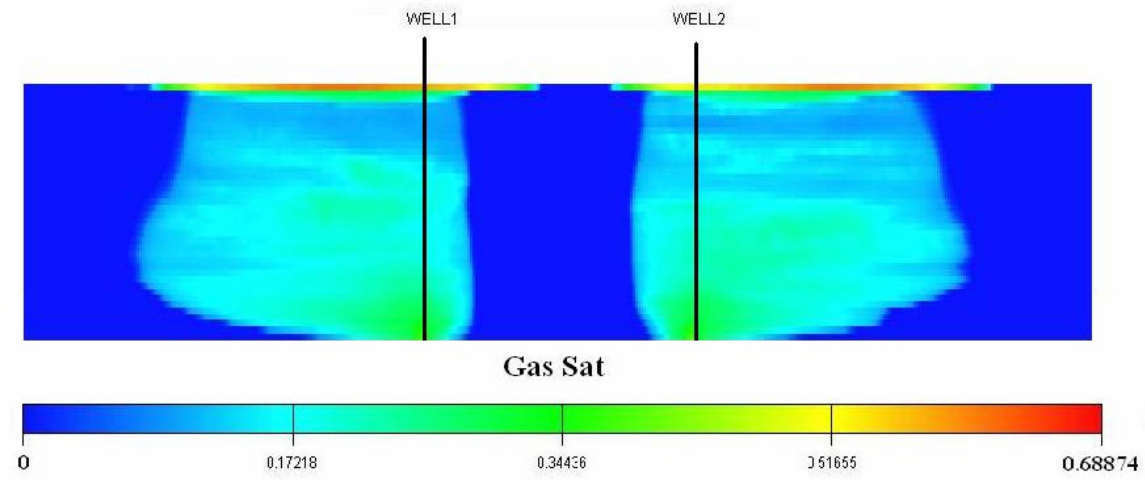


**Figure 4.8: Gas saturation distribution at the end of shut-in period (Case 4.3: base case)**

Optimization of the two-well case produced gas saturation distributions (Figure 4.9 and Figure 4.10) quite different from those obtained in the base case (Case 4.3). The optimized valve settings and the corresponding injection rates are presented in Table 4-3. For the first four optimization steps, the optimal valve settings stay essentially the same. A much larger amount of $CO_2$ is injected through well 2 as compared to well 1. This

difference is probably due to the heterogeneities in the reservoir. Low permeability regions around well 2 slow the vertical migration of $CO_2$ allowing more of the gas to travel laterally and thereby leading to higher residual trapping. However by the end of the fourth optimization step, a significant amount of $CO_2$ injected at well 2 appears near the top of the reservoir. This seems to be the reason why the optimization algorithm shuts down the well and injects all the gas from well 1.

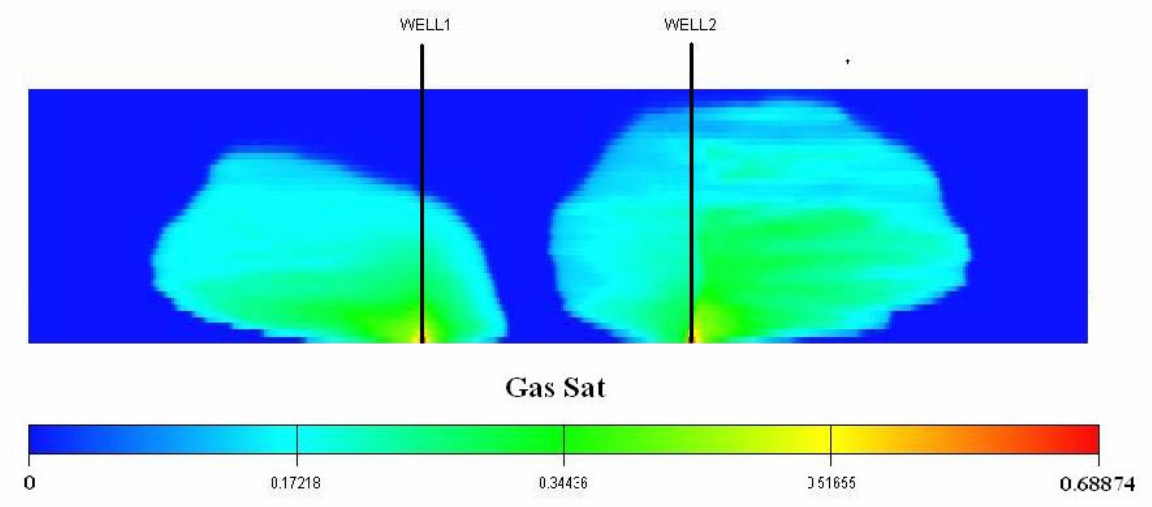


**Figure 4.9: Gas saturation distribution at the end of injection period (Case 4.4: optimized 2-well case)**

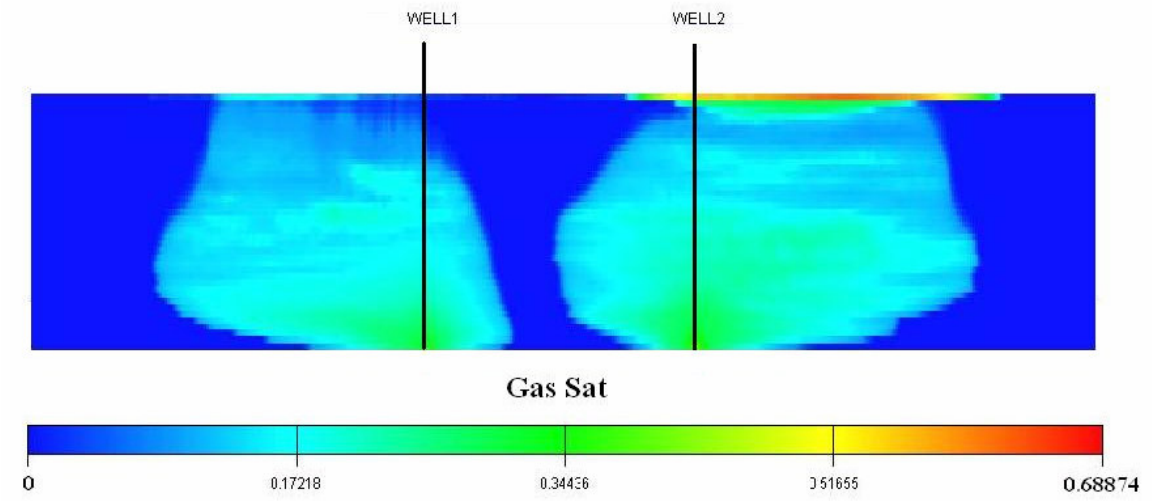


**Figure 4.10: Gas saturation distribution at the end of shut-in period (Case 4.4: optimized 2-well case)**

**Table 4-3: Valve Settings and Injection Rates for Case 4.4 (optimized 2-well case)**

| Time (up to) days | Valve #1 (well 1) | Valve #2 (well 2) | Injection Rate (well 1) mcf/d | Injection Rate (well 2) mcf/d |
|---|---|---|---|---|
| 730 | 30% Open | 91% Open | 1508 | 4492 |
| 1460 | 30% Open | 91% Open | 1501 | 4499 |
| 2190 | 30% Open | 91% Open | 1498 | 4502 |
| 2920 | 30% Open | 91% Open | 1508 | 4492 |
| 3650 | Fully Open | Fully Closed | 6000 | 0 |

The gas saturation in the topmost layer for the optimized two-well case (Case 4.4) was **0.2146** compared with **0.3754** in base case (Case 4.3). We therefore achieved an improvement of **~43%** over the unoptimized solution. The $CO_2$ saturation in the top layer for the optimized single-well case (Case 4.2) was **0.4421.** There was therefore an improvement of **~51%** when two wells (Case 4.4) were used instead of a single well (Case 4.2).

The effect of injection rates on residual trapping has been previously analyzed in various studies (mentioned earlier in Chapter 2). All the studies concluded that higher injection rates would lead to greater residual trapping of $CO_2$. The primary reason for this effect is that higher injection rates result in stronger viscous forces, so during the injection period the $CO_2$ displacement front travels further into the formation. Then, when the injection stops and the $CO_2$ migrates to the top under gravity forces, it comes into contact with a larger reservoir area, leading to greater residual trapping.

These results emphasize the importance of optimization of the injection rates and the number of wells in a $CO_2$ sequestration project. This is because, while increasing the number of wells increases the area of the reservoir exposed to $CO_2$ thereby increasing the residual trapping, it also results in lower injection rates for the wells. During the injection phase, low injection rates cause gravity effects to become stronger relative to viscous effects, which in turn cause a greater portion of the injected $CO_2$ to migrate upward rather

than moving laterally into the reservoir. This may lead to poor residual trapping. The gas injection rate effect is therefore a crucial factor to consider when determining the number of wells and the individual well injection rates.

### *4.2.3. Three-Well Case*

For this case, another well was introduced into the aquifer. This well was completed in the grid block (200, 1, 40), which is in the middle of the existing two wells. So, while there was well to well interaction, boundary effects were still weak. The total field injection rate was kept the same (6000 mcf/d).

For the base case (Case 4.5), equal injection rates were assigned to all the wells. The gas saturation distributions at the end of the injection period and at the end of shut-in period for this case are shown in Figures 4.11 and 4.12. The gas saturation in the top layer of the aquifer after the shut-in period was **0.2336** for the base case.

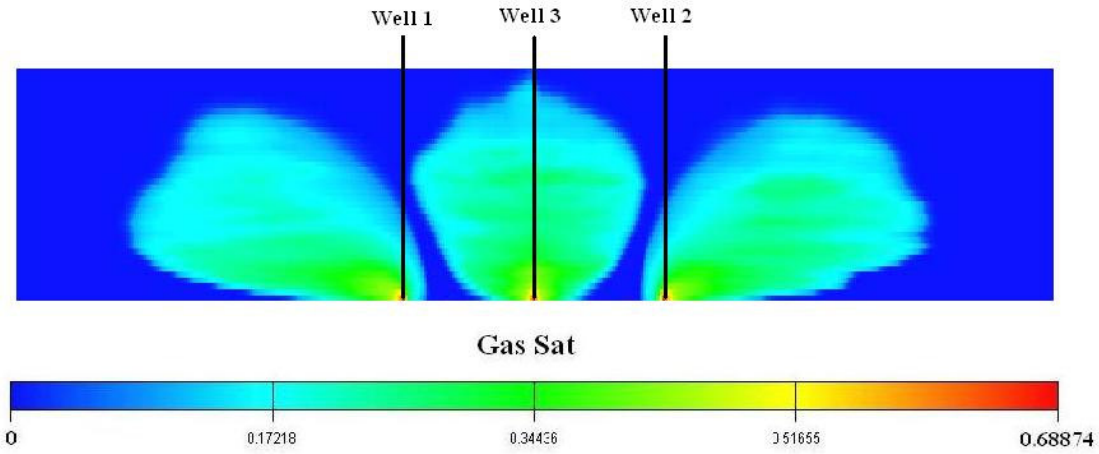


**Figure 4.11: Gas saturation distribution at the end of injection period (Case 4.5: 3-well base case)**

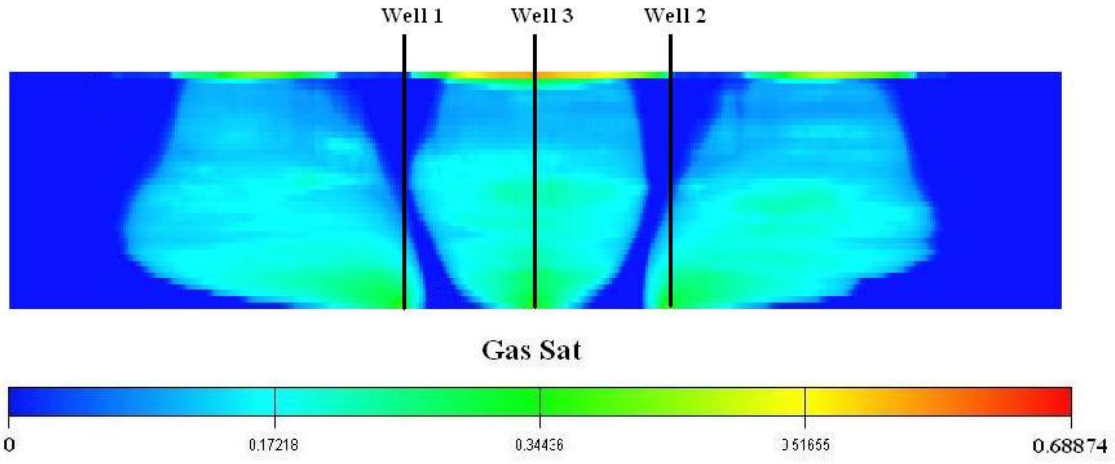


**Figure 4.12: Gas saturation distribution at the end of shut-in period (Case 4.5: 3-well base case)**

Again, carrying out optimization for the 3-well case increased the residual trapping in the reservoir. The gas saturation distributions (Figure 4.13 and Figure 4.14) are somewhat different from those for the base case (Case 4.5). The area of the reservoir contacted by the injected $CO_2$ is visibly larger for the optimized case (Case 4.6). This is probably the reason why we got more residual trapping for the optimized case (Case 4.6). The gas saturation in the top layer of the aquifer for the optimized case (Case 4.6) was reduced to **0.l46**, **~ 37.5%** less than the base case. The optimized valve settings and the corresponding injection rates are presented in Table 4-4.

**Table 4-4: Valve Settings and Injection Rates for Case 4.6 (optimized 3-well case)**

| Time (up to) days | Valve #1 (well 1) | Valve #2 (well 2) | Valve #3 (well 3) | Injection Rate (well 1) mcf/d | Injection Rate (well 2) mcf/d | Injection Rate (well 3) mcf/d |
|---|---|---|---|---|---|---|
| 730 | 68% Open | 64% Open | 100% Open | 1768.2 | 1658.2 | 2573.6 |
| 1460 | 67% Open | 64% Open | 100% Open | 1739.2 | 1661.5 | 2599.3 |
| 2190 | 64% Open | 63% Open | 100% Open | 1702.3 | 1650.7 | 2647 |
| 2920 | 71% Open | 57% Open | 100% Open | 1860 | 1513 | 2627 |
| 3650 | 100% Open | 75% Open | 100% Closed | 3423.7 | 2576.3 | 0 |

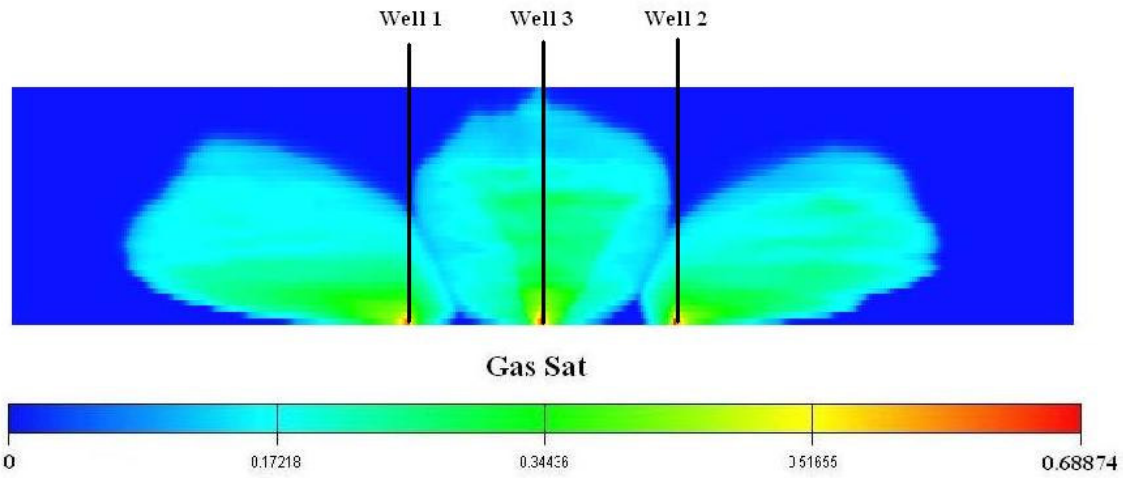


**Figure 4.13: Gas saturation distribution at the end of injection period (Case 4.6: optimized 3-well case)**

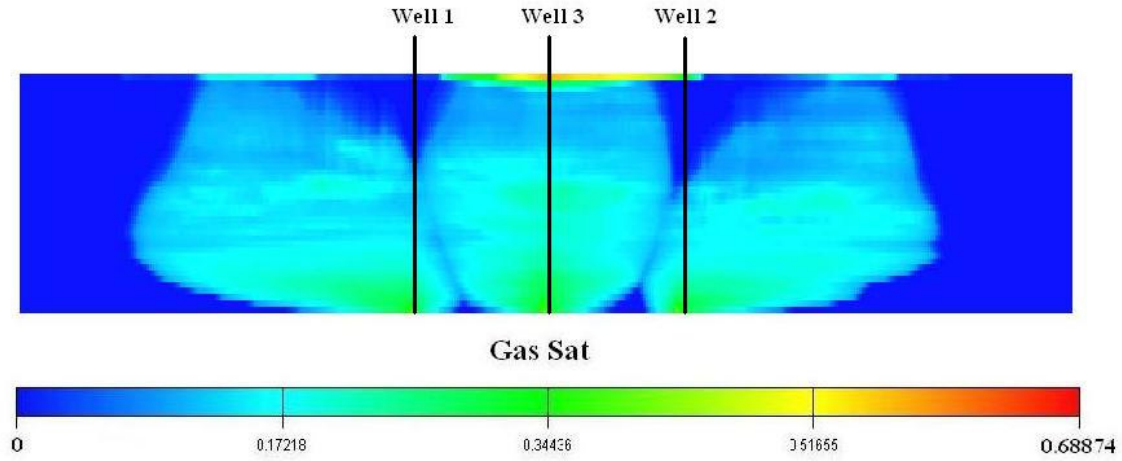


**Figure 4.14: Gas saturation distribution at the end of shut-in period (Case 4.6: optimized 3-well case)**

If we compare the gas saturation in the top layer for the optimized 3-well case (Case 4.6) with that of the optimized 2-well case (Case 4.4) and the optimized single-well case (Case 4.2), we see that we get more residual trapping for the 3-well case. For the optimized 3-well case (Case 4.6) the top layer gas saturation was **0.146**, while it was **0.2146** for the optimized 2-well case (Case 4.4) and **0.4421** for the optimized single-well case (Case 4.2). This result highlights the need for optimization of both the well injection rates and the number of wells for a $CO_2$ sequestration process.

### *4.2.4. Impact of Number of Optimization Steps*

For the cases considered above, the 10 year injection period was divided into 5 optimization steps. As discussed in Chapter 3, the current algorithm is not well suited for a large number of wells and optimization steps. A large number of optimization steps (and therefore smaller time periods between the changes in valve settings) should lead to better solutions, but at the cost of higher computational demands.

To estimate the impact of the number of optimization steps on the solution, we carry out optimization for the two-well case with 10 optimization steps (as opposed to 5 steps used in Case 4.4). The saturation distributions at the end of the injection period and at the end of shut-in period are shown in Figures 4.15 and 4.16. The optimized valve settings and the corresponding injection rates are presented in Table 4-5.

If we compare the valve settings obtained from a 10 step optimization (Case 4.7) with the 5 step optimization (Case 4.4), we see some significant changes. Overall, the optimization still accounts for the reservoir heterogeneities and injection rate effects. However, more $CO_2$ is injected through well 2 compared with well 1. Initially the valve settings for both the cases, Case 4.4 and Case 4.7, are more or less similar. However, gradually we see the differences in valve settings between the two cases becoming greater. Since more optimization steps provides the optimization algorithm with better control over the well injection rates, the algorithm shuts down well 2 after 2190 days in Case 4.7. For the case with 5 optimization steps (Case 4.4), the well was shut down after 2920 days. This results in very different gas saturation distributions for the two cases (Figures 4.10 and 4.16).

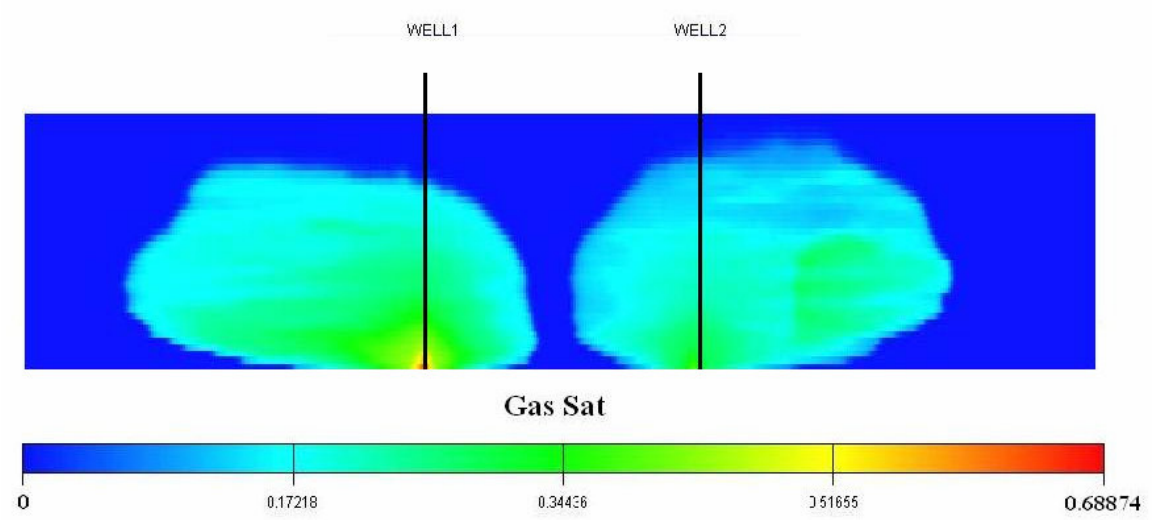


**Figure 4.15: Gas saturation distribution at the end of injection period (Case 4.7: optimized 2-well case with 10 optimization steps)**

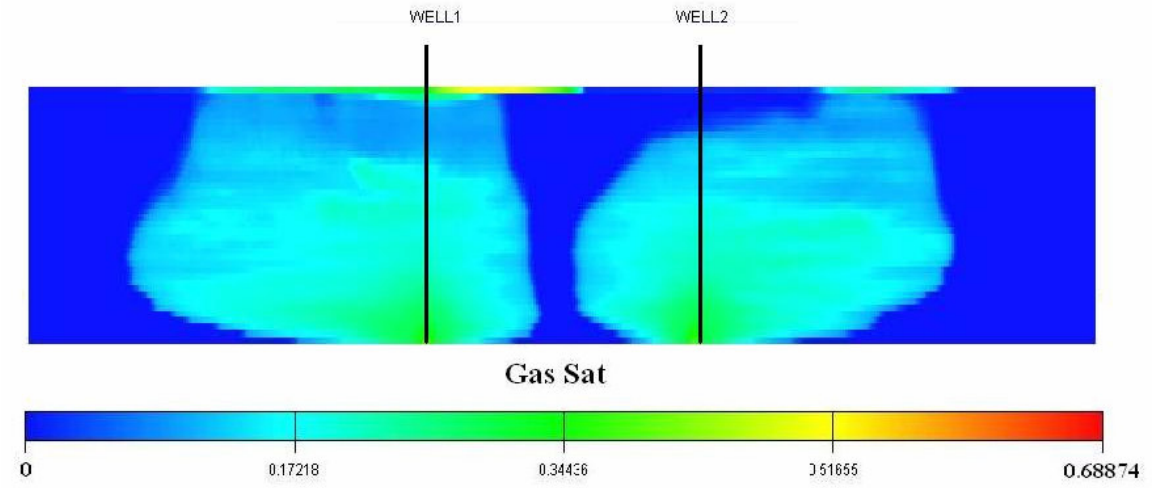


**Figure 4.16: Gas saturation distribution at the end of shut-in period (Case 4.7: optimized 2-well case with 10 optimization steps)**

The gas saturation in the topmost layer for Case 4.7 is **0.1527**, compared to **0.2146** in Case 4.4. There is an improvement of **~29%** over the previous solution and **~60%** over the base case (Case 4.3). This improvement however came at significant computational effort. More than 500 function evaluations (simulations) were needed in this case compared to approximately 200 function evaluations for the case with 5 optimization steps (Case 4.4).

**Table 4-5: Valve Settings and Injection Rates for Case 4.7 (optimized 2-well case with 10 optimization steps)**

| Time (up to) days | Valve #1 (well 1) | Valve #2 (well 2) | Injection Rate (well 1) mcf/d | Injection Rate (well 2) mcf/d |
|---|---|---|---|---|
| 365 | 29% Open | 88% Open | 1504 | 4496 |
| 730 | 29% Open | 88% Open | 1504 | 4496 |
| 1095 | 29% Open | 88% Open | 1505 | 4495 |
| 1460 | 28% Open | 88% Open | 1460 | 4540 |
| 1825 | 28% Open | 88% Open | 1434 | 4366 |
| 2190 | 26% Open | 85% Open | 1414 | 4586 |
| 2555 | Fully Open | Fully Closed | 6000 | 0 |
| 2920 | Fully Open | Fully Closed | 6000 | 0 |
| 3285 | Fully Open | Fully Closed | 6000 | 0 |
| 3650 | Fully Open | Fully Closed | 6000 | 0 |

### *4.2.5. Capillary Pressure*

As mentioned in Chapter 1, hysteresis effects are observed in both relative permeability and capillary pressure functions. Therefore it is expected that accounting for capillary pressure would increase the residual trapping of $CO_2$. Capillary pressure was neglected in the previous simulations since including it did not affect the gas saturation distribution in the base cases significantly (this was ascertained by running simulations with and without capillary pressure). However, as we will see, including capillary pressure may affect the valve settings determined by the optimization procedure.

The capillary pressure ($P_{cap}$) function for drainage was generated using the van Genuchten (1980) formulation:

$$P_{cap} = -P_0 \left( \left[ S^* \right]^{-1/\lambda} - 1 \right)^{1-\lambda} \tag{4.1}$$

$$S^* = (S_w - S_{wr})/(1 - S_{wr}) \tag{4.2}$$

where,

$S_{wr}$ = 0.31 (irreducible water saturation)

$\lambda$ = 5 (exponent)

$P_0$ = 0.1961 bars (strength coefficient)

We used the capillary pressure curve for imbibition presented previously by Ide *et al.* (2007), adjusted for the end point saturation values. The generated curves are shown in Figure 4.17.

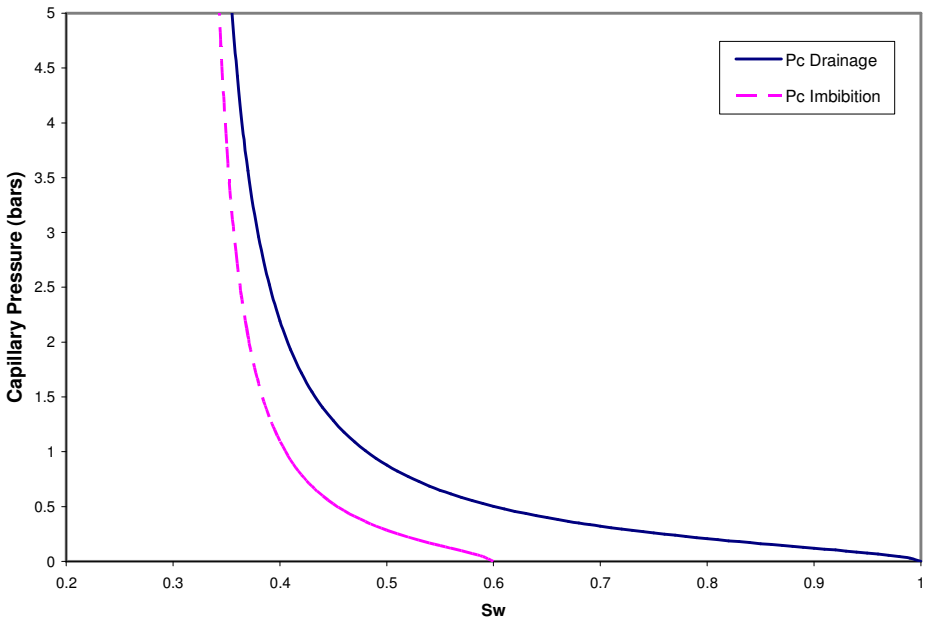


**Figure 4.17: Capillary pressure curves**

For the two-well base case (Case 4.8), the same amounts of $CO_2$ were injected through the two wells and capillary pressure effects were included in the simulation (unlike in Case 4.3). The gas saturation distributions are shown in Figure 4.18 and Figure 4.19. The gas saturation in the topmost layer after the shut-in period was **0.3757** as compared to **0.3754** for Case 4.3 (without capillary pressure).

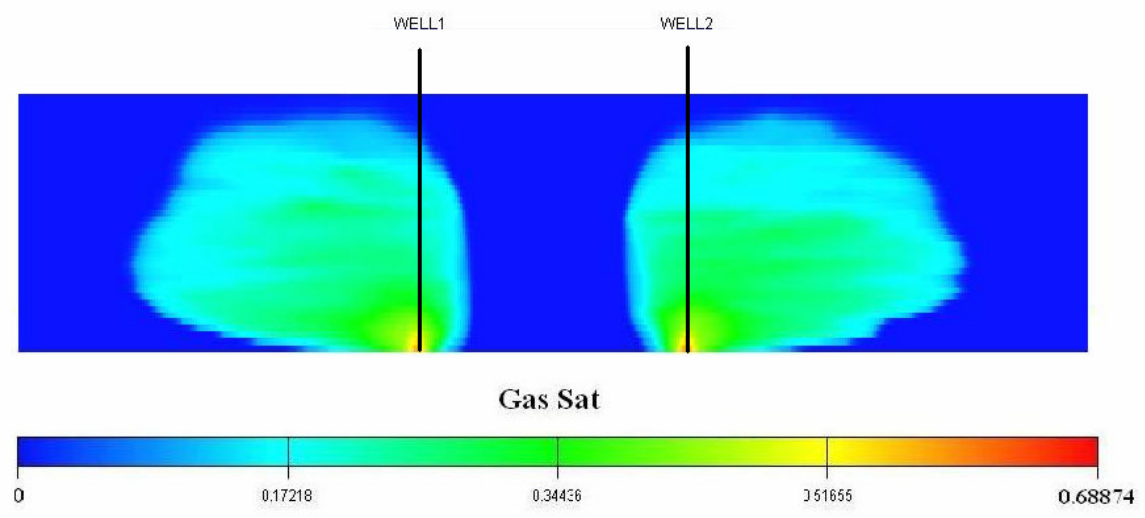


**Figure 4.18: Gas saturation distribution at the end of injection period (Case 4.8: base case with capillary pressure hysteresis)**

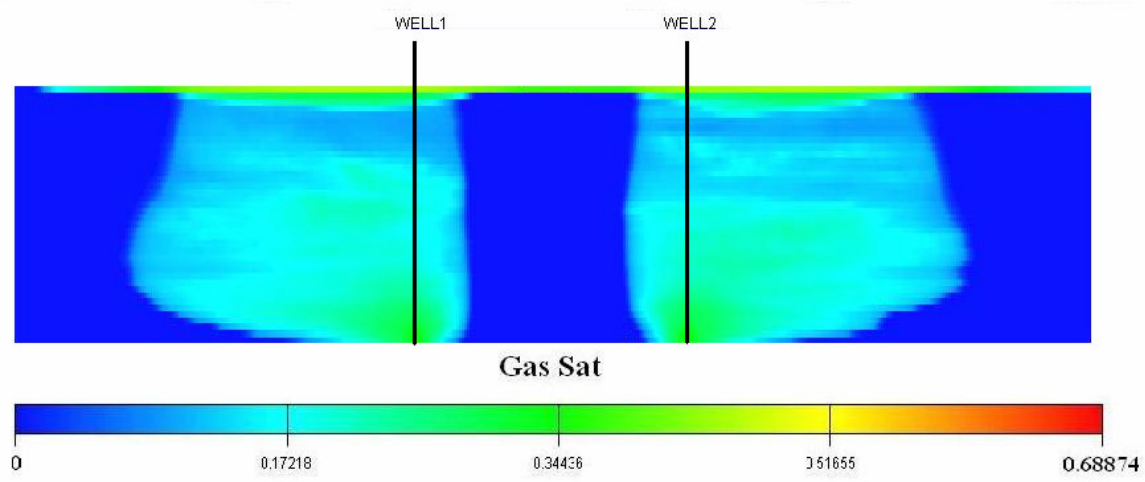


**Figure 4.19: Gas saturation distribution at the end of shut-in period (Case 4.8: base case with capillary pressure hysteresis)**

The gas saturation distributions for the optimized case at the end of the injection period and the end of shut-in period are shown in Figures 4.20 and 4.21. The average gas saturation of the topmost layer was **0.2066** (as compared to **0.2146** for the optimized two-well case without capillary pressure). If we compare the valve settings obtained for Case 4.9 with those obtained for Case 4.4 (optimized two-well case without the capillary pressure effect), they are however quite different. For Case 4.4 most of the gas was injected from well 2 during the first 4 optimization periods. Here, in Case 4.9, most of the gas is being injected through well 1 for the first 4 time steps. The valve settings and injection rates are given in Table 4-6.

**Table 4-6: Valve Settings and Injection Rates for Case 4.9**

| Time (up to) days | Valve #1 (well 1) | Valve #2 (well 2) | Injection Rate (well 1) mcf/d | Injection Rate (well 2) mcf/d |
|---|---|---|---|---|
| 730 | 33% Open | 100% Open | 1507 | 4493 |
| 1460 | 37% Open | 8.5% Open | 4864 | 1136 |
| 2190 | 37% Open | 8% Open | 4905 | 1095 |
| 2920 | 37% Open | 7% Open | 4950 | 1050 |
| 3650 | Fully Closed | Fully Open | 0 | 6000 |

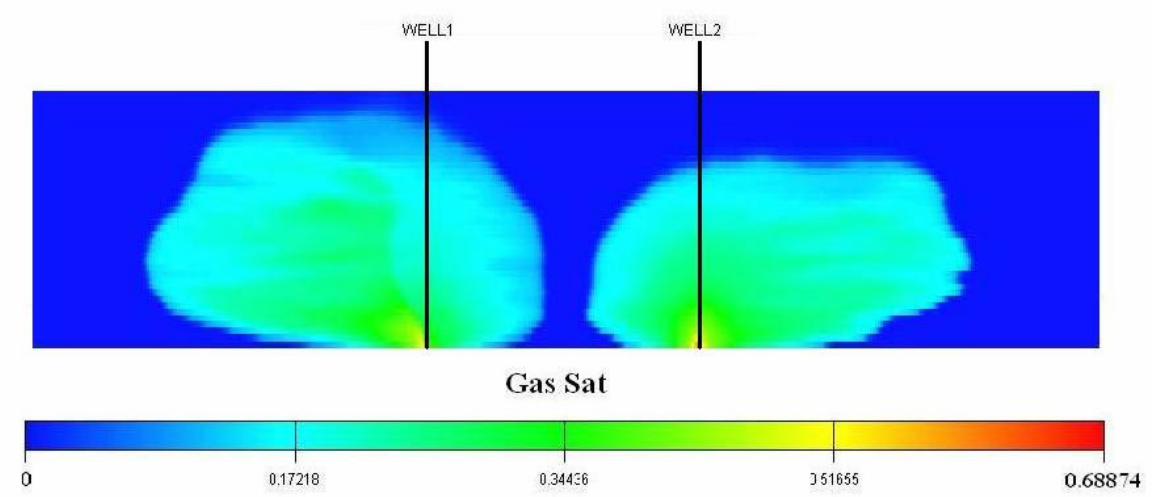


**Figure 4.20: Gas saturation distribution at the end of injection period (Case 4.9: optimized 2-well case with capillary pressure hysteresis)**

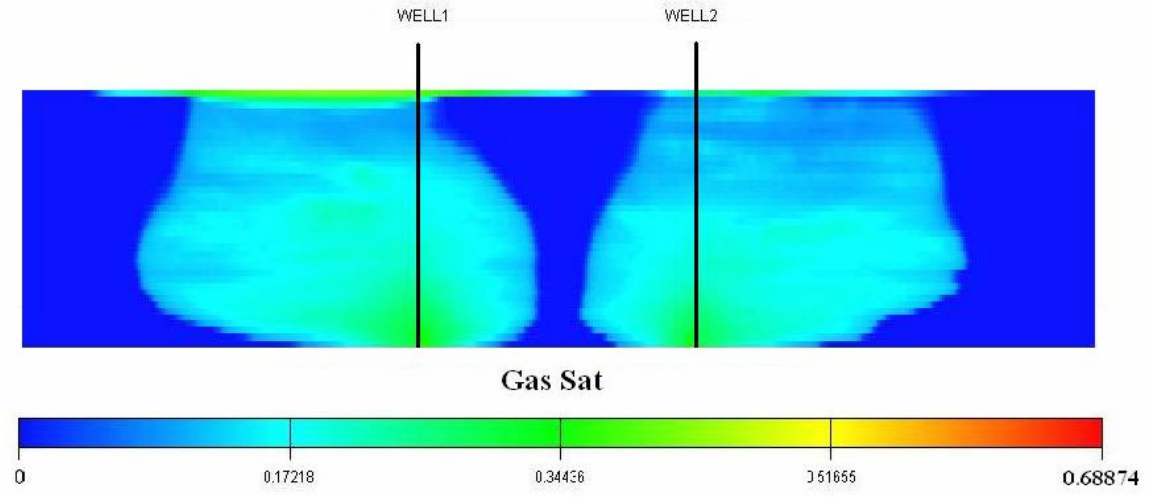


**Figure 4.21: Gas saturation distribution at the end of shut-in period (Case 4.9: optimized 2-well case with capillary pressure hysteresis)**

Comparing the results for the base cases with and without capillary pressure effects (Case 4.8 and Case 4.3), the gas saturation distribution is seen to be a bit different. If we look closely at the results for the two cases at the end of injection period (Figure 4.7 and Figure 4.18), we can see that the gas saturation within the $CO_2$ plume for the case without capillary pressure (Case 4.3) is higher than that in the case with capillary pressure (Case 4.8). This is because the presence of capillary pressure reduces the maximum gas saturations reached prior to the imbibition phase in the reservoir and thus limits the amount of residual trapping (Ide *et al*., 2007; Mo and Akervoll, 2005). At the end of the shut-in period, the amount of structurally trapped $CO_2$ is essentially the same for the two cases (0.3754 for Case 4.3 and 0.3757 for Case 4.8). The distribution of gas in the top layer is however different for the two cases (Figure 4.8 and Figure 4.19). The reason for this could be that in the case with capillary pressure (Case 4.8), during the long shut-in period the brine imbibes into the gravity tongue at the top of the aquifer, thereby spreading and reducing the gas saturation (Figure 4.19 and Figure 4.21). It is important to note here that this process leads to trapping of $CO_2$ even in the top layer of the aquifer, offsetting the reduction in the trapped $CO_2$ (Ide *et al.*, 2007). The trapped $CO_2$ in the top layer has not been accounted for in this study (since we assume the $CO_2$ in the top layer to be mobile, as was the case in all previous simulations).

The differences in valve settings in the optimized cases (Case 4.9 and Case 4.4) may be due to the effect of capillary pressure on the imbibition process in regions of low permeability. They may also just reflect the non-uniqueness inherent in the optimization (due to convergence to a local rather than global minimum). These results do suggest that capillary pressure and capillary pressure hysteresis should be accounted for in the simulation model used for optimization. For the case considered here, including the capillary pressure did not result in a significant difference in the optimized objective function, though it could make a difference under different conditions.

### *4.2.6. Effect of Heterogeneity*

All of the results presented so far in this chapter were for a mildly heterogeneous aquifer (Figure 4.1). In this section, simulations were carried out for the 2-well case using two new models with greater heterogeneity. These models were generated in the same way as the previous model using the same variogram parameters. However, the standard deviation of log permeability (*logk*) for the two models was 1 and 2, instead of 0.3 (used in the previous model). For convenience, from here on we will refer to the previous model as "Model 1," the model with $\sigma_{logk}$=1 as "Model 2" and the model with $\sigma_{logk}$=2 as "Model 3." The permeability fields for Model 2 and Model 3 are shown in Figure 4.22 and Figure 4.23. The values of $k_v/k_h$ were 0.2 and 0.5 for Model 2 and Model 3 respectively. Finally, the boundary conditions for these models are the same as those in Model 1. In these cases we inject 5000 mcf/d (rather than 6000 mcf/d as in the previous cases).

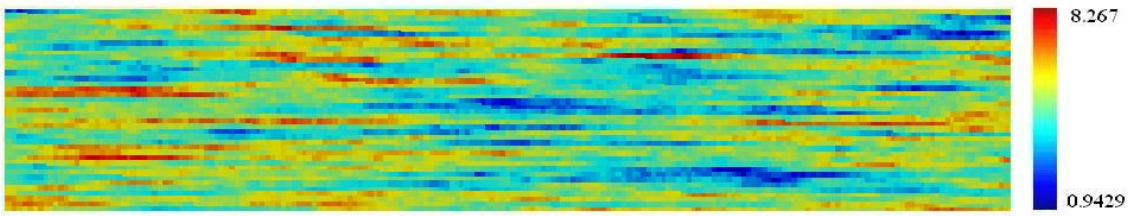


**Figure 4.22: Log Permeability (*log k*) field for Model 2**

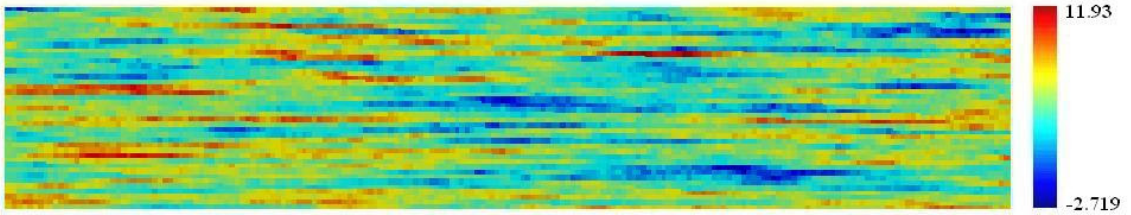


**Figure 4.23: Log Permeability (*log k*) field for Model 3**

## Model 2

First, we will discuss the optimization of the 2-well case for Model 2. For the base case (Case 4.10), the two injection wells were operated at equal rates. The gas saturation distributions in the aquifer at the end of the injection period and at the end of the shut-in period are shown in Figure 4.24 and Figure 4.25.

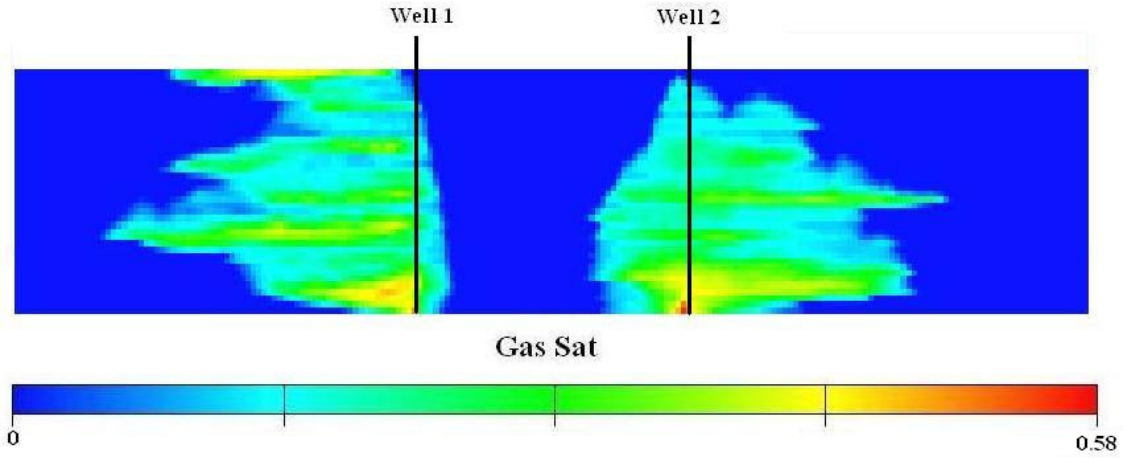


**Figure 4.24: Gas saturation distribution at the end of injection period (Case 4.10: 2-well base case with Model 2)**

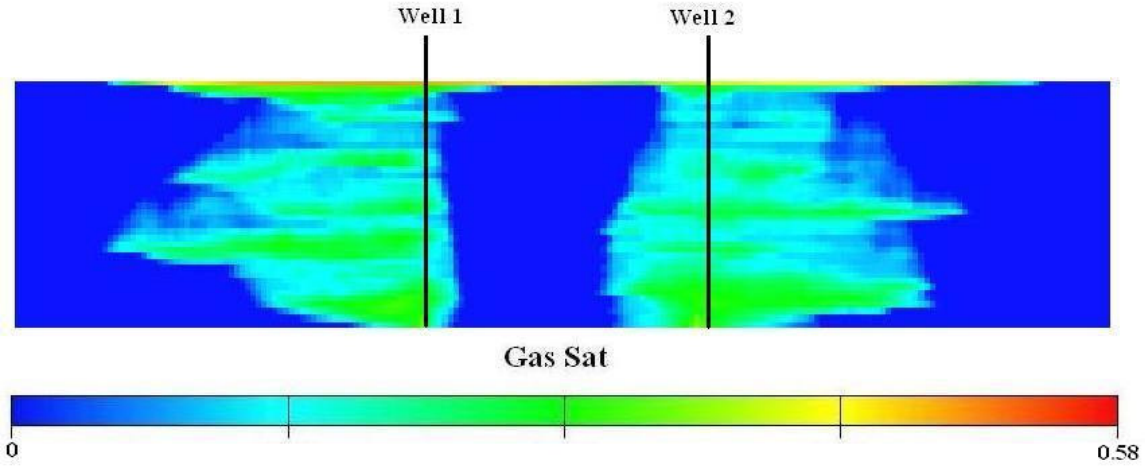


**Figure 4.25: Gas saturation distribution at the end of shut-in period (Case 4.10: 2-well base case with Model 2)**

As we can see from the Figure 4.22, there are regions of low permeability around well 2. As a result, when we inject equal amounts through both wells, we see from Figures 4.24 and 4.25 that a large portion of the gas injected at well 1 reaches the top of the aquifer as a mobile phase while the gas injected at well 2 undergoes greater residual trapping. The gas saturation in the top layer of the aquifer for the base case (Case 4.10) was **0.3492.**

Optimization was then carried out for the 2-well case with Model 2. The gas saturation distributions for the optimized 2-well case (Case 4.11) at the end of the injection period and at the end of the shut-in period are shown in Figures 4.26 and 4.27. The optimized

valve settings are given in Table 4-7. The average top layer gas saturation for the optimized case (Case 4.11) was **0.275**. There was therefore a reduction of **~21%** in the amount of gas that is structurally trapped.

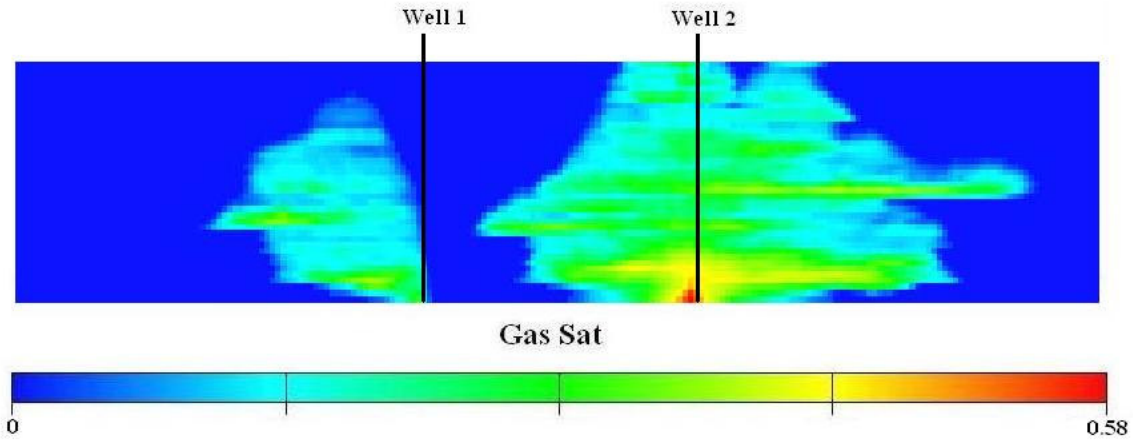


**Figure 4.26: Gas saturation distribution at the end of injection period (Case 4.11: 2-well optimized case with Model 2)**

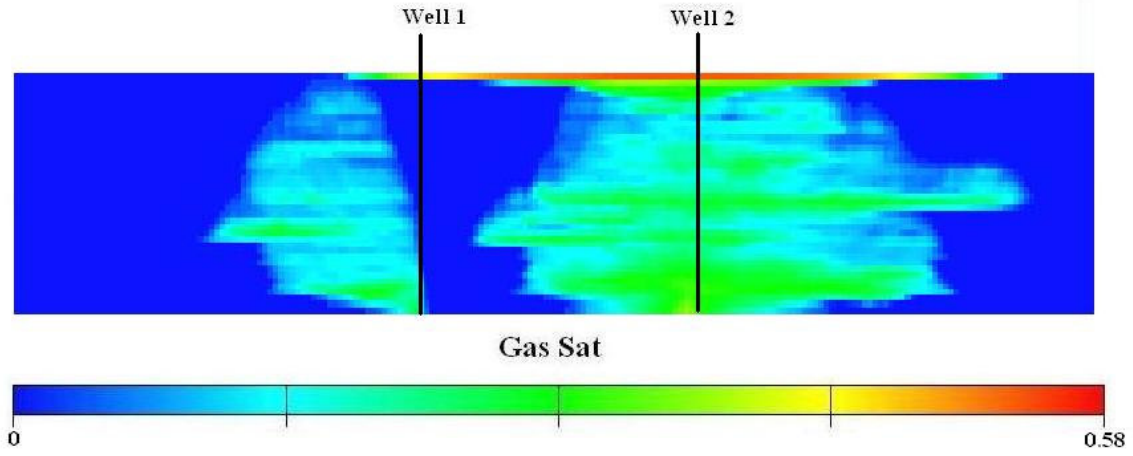


**Figure 4.27: Gas saturation distribution at the end of shut-in period (Case 4.11: 2-well optimized case with Model 2)**

From Table 4-7 we see that the optimal valve settings for the two-well optimized case for Model 2 remained essentially the same over the 5 optimization steps. Most of the gas was injected from well 2, with just a small portion of it being injected from well 1.

**Table 4-7: Valve Settings and Injection Rates for Case 4.11**

| Time (up to) days | Valve #1 (well 1) | Valve #2 (well 2) | Injection Rate (well 1) mcf/d | Injection Rate (well 2) mcf/d |
|---|---|---|---|---|
| 730 | 21% Open | 92% Open | 953 | 4047 |
| 1460 | 21% Open | 92% Open | 953 | 4047 |
| 2190 | 21% Open | 92% Open | 953 | 4047 |
| 2920 | 21% Open | 92% Open | 953 | 4047 |
| 3650 | 16% Open | 91% Open | 778 | 4222 |

## Model 3

Now, we look at the results for the optimization of the two-well case with Model 3. For the base case (Case 4.12), the injection rates were kept equal for the two wells. The gas saturation distributions in the aquifer at the end of the injection period and at the end of the shut-in period are shown in Figure 4.28 and Figure 4.29. The average gas saturation in the top layer for the base case was **0.2158**.

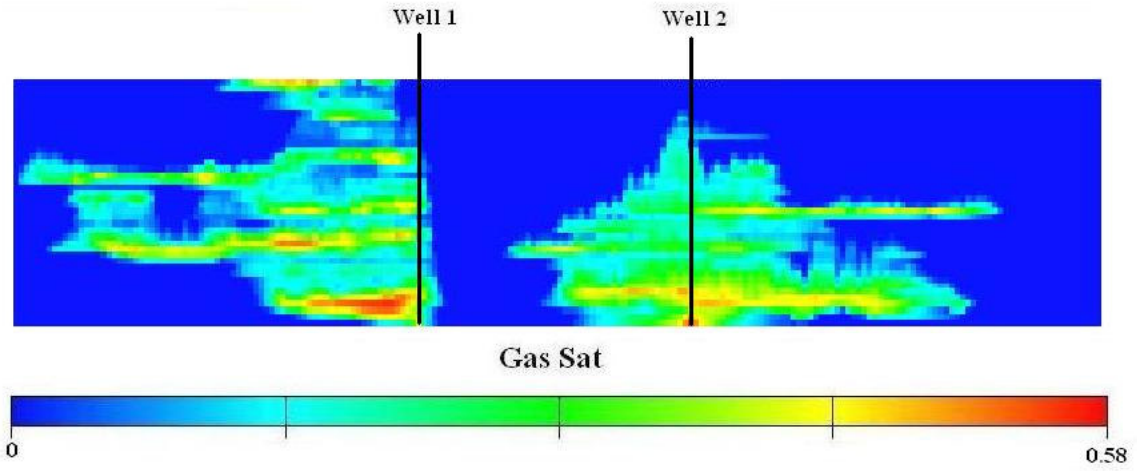


**Figure 4.28: Gas saturation distribution at the end of injection period (Case 4.12: 2-well base case with Model 3)**

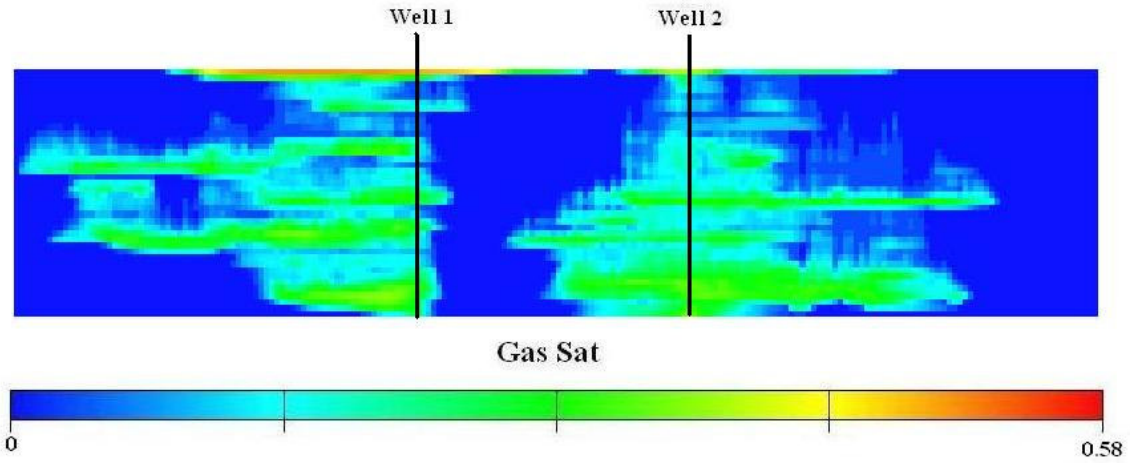


**Figure 4.29: Gas saturation distribution at the end of shut-in period (Case 4.12: 2-well base case with Model 3)**

Optimization of the 2-well case with Model 3 (Case 4.13) gave a gas saturation of **0.1737** in the top layer of the aquifer. This was a decrease of ~19.5% over the base case (Case 4.12) gas saturation. Again, the optimal valve settings for the 5 optimization steps remained essentially the same for this case (Case 4.13), with most of the gas again being injected through well 2. The gas saturation distributions for the optimized case (Case 4.13) at the end of the injection and shut-in periods are given in Figures 4.30 and 4.31. The optimal vale settings are given in Table 4-8.

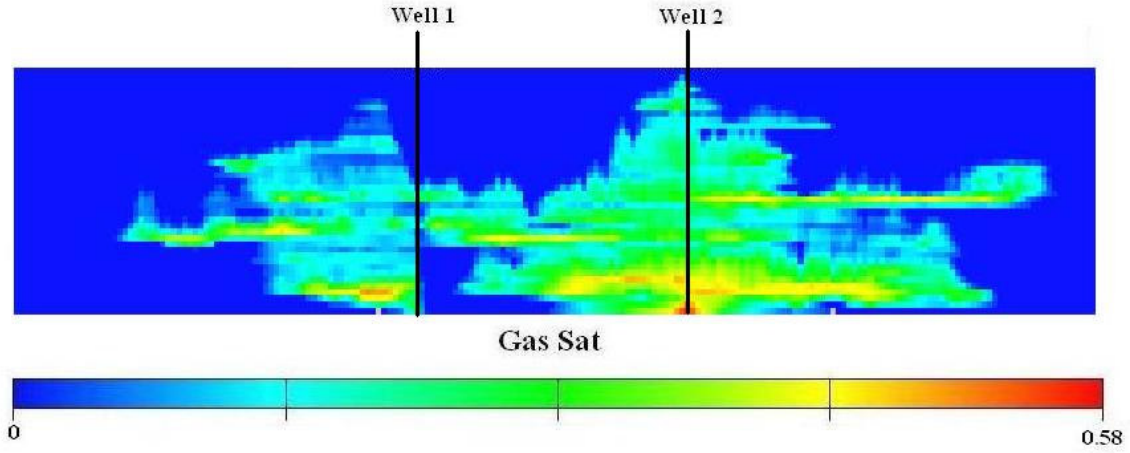


**Figure 4.30: Gas saturation distribution at the end of injection period (Case 4.13: 2-well optimized case with Model 3)**

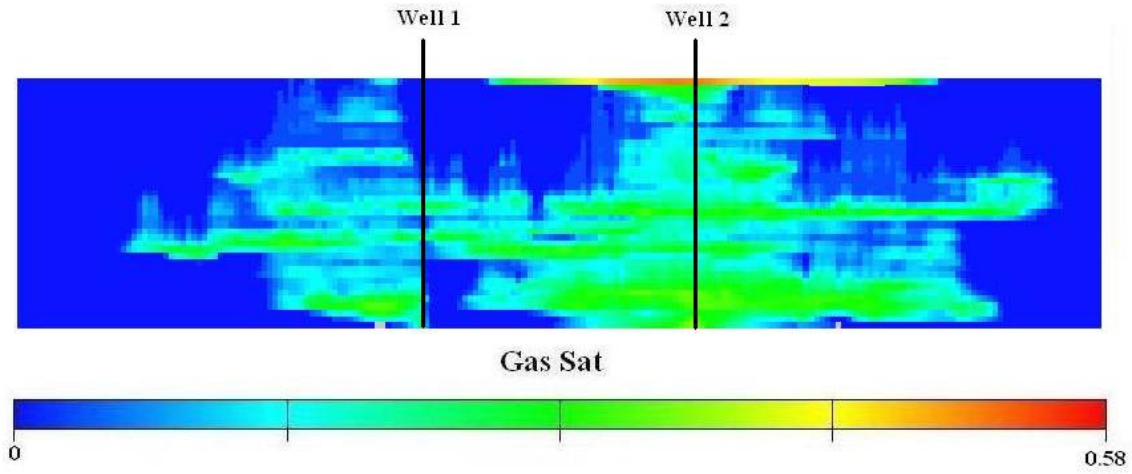


**Figure 4.31: Gas saturation distribution at the end of shut-in period (Case 4.13: 2-well optimized case with Model 3)**

**Table 4-8: Valve Settings and Injection Rates for Case 4.13**

| Time (up to) days | Valve #1 (well 1) | Valve #2 (well 2) | Injection Rate (well 1) mcf/d | Injection Rate (well 2) mcf/d |
|---|---|---|---|---|
| 730 | 16.4% Open | 58% Open | 1115 | 3885 |
| 1460 | 16.8% Open | 58% Open | 1125 | 3875 |
| 2190 | 16.8% Open | 58% Open | 1125 | 3875 |
| 2920 | 16.8% Open | 58% Open | 1125 | 3875 |
| 3650 | 16.8% Open | 58% Open | 1123 | 3877 |

The essentially constant injection rates observed for Models 2 and 3 are somewhat surprising. This may be due to the algorithm not being fully converged or finding a local optimum. We next briefly consider some algorithmic issues.

## 4.3. Impact of Initial Settings on Optimization Results

The optimization results obtained for the last two cases (Case 4.11 and Case 4.13) indicate that the improvement in the solution is not as much as it was in the mildly heterogeneous reservoir (Model 1). Looking at the optimized valve settings, we observe basically no change in the valve settings. From the previously optimized cases with Model 1, we had observed some variation in the optimal valve settings, particularly at the end of the optimization period. So, it is possible that for the more heterogeneous cases, the solution surface is not as smooth, and the optimization algorithm is converging to a local minimum. If this is the case, we would require multiple runs of the algorithm with different initial values for the valve settings to achieve the optimal solution. It is also possible that a modified optimization algorithm (with for example another loop) might provide better results.

We tried to further improve the solutions obtained in Case 4.11 and Case 4.13 by running the algorithm a second time. This time we changed the initial valve settings (at each optimization step) to values we expected to be near the optimum (based on our observations for Model 1). From the first run of the algorithm, we saw (Table 4-7 and Table 4-8) that for both Model 2 and Model 3 the optimal solution was to inject at a much higher rate from well 2 than from well 1. However, saturation distributions (Figure 4.27 and Figure 4.31) for the optimized cases (Case 4.11 and Case 4.13) showed that a large amount of gas injected from well 2 was reaching the top while a very small amount of gas injected from well 1 ended up in the top layer. It was therefore decided to prescribe values close to the optimal valve settings obtained from the first run as the initial valve settings for the first 4 optimization steps, while for the last step, we gave initial settings that specify that most of the injected gas would be injected through well 1 instead of well 2 (in accordance with optimal valve settings for cases with Model 1).

The optimized valve settings obtained for Case 4.11 and Case 4.13 (with initial settings as described above) are given in Table 4-9 and Table 4-10 respectively. For Model 2, the average gas saturation of the top layer of the aquifer was **0.3492** for the base case (Case

4.10). This was reduced to **0.275** in the first optimization run (Case 4.11). We managed to further reduce it to **0.217** with the second optimization run. For Model 3, the gas saturation in the top layer was **0.2158** for the base case (Case 4.12). The saturation was reduced to **0.1737** with the first run of the optimization (Case 4.13) and then further reduced to **0.1397** with the second run.

**Table 4-9: Valve Settings and Injection Rates for Case 4.11 (Model 2, 2nd optimization run)**

| Time (up to) days | Valve #1 (well 1) | Valve #2 (well 2) | Injection Rate (well 1) mcf/d | Injection Rate (well 2) mcf/d |
|---|---|---|---|---|
| 730 | 21% Open | 92% Open | 939 | 4061 |
| 1460 | 21% Open | 92% Open | 924 | 4076 |
| 2190 | 21% Open | 92% Open | 953 | 4047 |
| 2920 | 21% Open | 92% Open | 944 | 4056 |
| 3650 | 100% Open | 100% Closed | 5000 | 0 |

**Table 4-10: Valve Settings and Injection Rates for Case 4.13 (Model 3, 2nd optimization run)**

| Time (up to) days | Valve #1 (well 1) | Valve #2 (well 2) | Injection Rate (well 1) mcf/d | Injection Rate (well 2) mcf/d |
|---|---|---|---|---|
| 730 | 16.4% Open | 58% Open | 1115 | 3885 |
| 1460 | 16.8% Open | 58% Open | 1126 | 3874 |
| 2190 | 16.8% Open | 58% Open | 1126 | 3874 |
| 2920 | 16.8% Open | 58% Open | 1126 | 3874 |
| 3650 | 100% Open | 100% Closed | 5000 | 0 |

These results show that the algorithm was indeed providing sub-optimal well settings during the first run of the algorithm and that we can achieve appreciable improvement in

the solution with a second run. However this is still probably not the global minimum. Multiple runs of the algorithm might therefore be required to obtain the optimum solution.

# Chapter 5

# 5. Conclusions and Future Work

## 5.1. Summary and Conclusions

In this report we extended the application of well control optimization to $CO_2$ sequestration processes. The optimization procedure utilized a previously developed smart well optimization method based on a defensive control strategy. In this method, the valve settings were determined by optimizing an objective function over the current optimization step and the entire remaining simulation period, using numerical gradients and a conjugate gradient (CG) algorithm. In this work, we modified the objective function and the optimization algorithm so that it could be applied to $CO_2$ sequestration problems with multiple wells. The objective of the optimizations was to minimize the amount of structurally trapped $CO_2$ (maximize residually trapped $CO_2$).

The benefits of optimization for a variety of cases were investigated. These cases were designed to assess the effect of factors such as aquifer heterogeneity, number of wells, and capillary pressure on the residual trapping of the injected $CO_2$. Our specific conclusions are as follows:

- In all of the cases, the optimization procedure increased the amount of residual trapping over the base cases by an appreciable amount. In the two-well case, the optimized solution had ~43% lower gas saturation at the top of the aquifer than in the unoptimized solution. For the three-well case, optimization produced a ~37.5% decrease in the gas saturation reaching the top of the aquifer over the base (unoptimized) case.

- The effect of increasing the number of optimization steps on the optimized solution was also assessed. Upon increasing the optimization steps from 5 to 10, the gas saturation in the top layer decreased from 0.2146 to 0.1527 for the two-well case. This improvement however came at a cost of significant increase in computational requirements.
- The valve settings obtained were different depending on whether or not capillary pressure was included in the simulations, though there was not a significant difference between the optimized solutions in terms of residually trapped $CO_2$. It is not clear if this difference was due to capillary pressure hysteresis or due to the optimization algorithm converging to a different optimal solution. More study is needed to understand this effect.
- Increased heterogeneity resulted in optimized solutions with essentially constant valve settings. This could be due to the convergence of the optimization algorithm to a sub-optimal solution.
- Running the optimization with different initial settings for the models with high heterogeneity produced improved results, confirming that the solutions obtained previously were not the optimal solutions. Further investigation of this issue is required.

## 5.2. Recommendations for Future Work

The optimization procedure used in this study computed the function gradients numerically, using a commercial simulator as a "black box." The next step would be to use an adjoint method for optimization of $CO_2$ sequestration processes. Work has been done to enhance Stanford's General Purpose Research Simulator (GPRS) to include additional effects important for $CO_2$ sequestration simulations (Fan, 2006). The adjoint method integrated with GPRS (Sarma *et al*., 2006) could be extended as required to provide a more accurate and computationally more efficient optimization procedure. Other optimization procedures could also be investigated.

# Nomenclature

| | |
|---|---|
| **b** | arbitrary vector |
| $C$ | Land's trapping coefficient |
| **d** | optimization search direction |
| **e** | set of unit vectors (identity matrix) |
| $F$ | objective function |
| $f$ | recovery factor |
| **g, G** | gradient vectors |
| **H** | Hessian matrix |
| $H$ | height of the reservoir |
| $h$ | objective function derivative step size |
| $k$ | permeability |
| $k_r$ | relative permeability |
| $k_{rg}$ | relative permeability of gas or non-wetting phase |
| $k_{rw}$ | relative permeability of water or wetting phase |
| $L$ | length of the reservoir |
| $P$ | pressure |
| $P_{cap}$ | capillary pressure |
| **r** | residual vector |
| $S$ | saturation |
| $S_g$ | gas (non-wetting phase) saturation |
| $S_{gi}$ | initial gas (non-wetting phase) saturation |

$S_{gmax}$ maximum gas (non-wetting phase) saturation

$S_{gt}$ trapped gas (non-wetting phase) saturation

$S_{gtmax}$ maximum trapped gas (non-wetting phase) saturation

$S_w$ water (wetting phase) saturation

$S_{wi}$ irreducible water (wetting phase) saturation

$u$ average flow velocity

$\mathbf{x}$ scaled vector of valve settings

## Supercripts

$k$ iteration level

$0$ initial value

## Subscripts

*cap* capillary

*g* gas

*h* horizontal

*i* initial

*min* minimum

*max* maximum

*s* solution

*v* vertical

*w* water

## Greek Symbols

| | |
|---|---|
| $\alpha$ | step size in search direction |
| $\beta$ | Gram-Schmidt constant |
| $\varepsilon$ | convergence factor |
| $\phi$ | porosity |
| $\gamma$ | specific gravity |
| $\lambda$ | Van Genuchten exponent |
| $\mu$ | viscosity |
| $\rho$ | density |

## Abbreviations

| | |
|---|---|
| CG | conjugate gradient |
| bbl/d | barrels per day |
| BHP | bottom hole pressure |
| mcf/d | thousand standard cubic feet per day |
| PV | pore volume |
| $rft^3/ft^3$ | reservoir cubic feet / standard cubic feet |

# References


Aitokhuehi, I., 2005, "Real-Time Optimization of Smart Wells," M.S. report, Department of Petroleum Engineering, Stanford University, California.

Aitokhuehi, I., and Durlofsky, L. J., 2005, "Optimizing the Performance of Smart Wells in Complex Reservoirs Using Continuously Updated Geological Models," *J. Petroleum Science and Engineering*, 48(2005), 254-284.

Al-Futaisi, A., and Patzek, T. W., 2003, "Impact of Wettability on Two-Phase Flow Characateristics of Sedimentary Rock: A Quasi-Static Description," *Water Resour. Res.*, 39(2), 1042, DOI: 10.1029/2002WR001366.

Brouwer, D. R., and Jansen, J. D., 2002, "Dynamic Optimization of Water Flooding with Smart Wells Using Optimal Control Theory," paper SPE 78278 presented at the SPE European Petroleum Conference, Aberdeen, UK, October 29-31.

Bryant, S. L., Lakshminarasimhan, S., and Pope G. A., 2006, "Buoyancy-Dominated Multiphase Flow and Its Impact on Geological Sequestration of $CO_2$," paper SPE 99938 presented at SPE/DOE Symposium on Improved Oil Recovery, Tulsa, April 22–26.

Dolle, N., Brouwer, D. R., and Jansen, J. D., 2002, "Dynamic Optimization of Water Flooding with Multiple Injectors and Producers Using Optimal Control Theory," paper presented at the XV International Conference on Computational Methods in Water Resources, Delft, Netherlands, June 23-28.

Energy Information Administration Website: U.S. Emissions Data, May 2007. Link: *http://www.eia.doe.gov/environment.html*.

Ennis–King, J., Online $CO_2$/Brine Property Calculator. Available through GEODISC: *http://www.apcrc.com.au/Programs/geodisc_res.html*, 2006.

Fan, Y., 2006, "Development of $CO_2$ Sequestration Modeling Capabilities in Stanford General Purpose Research Simulator," M.S. report, Department of Petroleum Engineering, Stanford University, California.

Friedmann, J., and Herzog, H., 2006, "Chapter 4: Geological Carbon Sequestration," MIT Report: Future of Coal in Carbon Constrained World, June 19.

Gale, J., 2002, "Overview of Sources, Potential, Transportation and Geological Distribution of Storage Possibilities," Presentation at IPCC Workshop on Carbon Capture and Storage, Regina, Canada, November 18-21.

GeoQuest. Eclipse Technical Description. *Schlumberger Geoquest Manual*, 2005a.

Ide, S. T., Jessen, K., and Orr, F. M., Jr., 2007, "Time Scales for Migration and Trapping of $CO_2$ in Saline Aquifers," accepted, *J. Greenhouse Gas Control*.

Izgec, O., Demiral, B., Bertin, H., and Akin A., 2005, "Experimental and Numerical Investigation of Carbon Sequestration in Saline Aquifers," paper SPE 94697 presented at the SPE/EPA/DOE Exploration and Production Environmental Conference, Galveston, March 7-9.

Jansen, J. D., Brouwer, D. R., Naevdal, G., and van Kruijsdiik, C. P. J. W., 2005, "Closed-Loop Reservoir Management," *First Break*, 23, 43-48, 2005.

Janssen, P. H., and Bossie-Codreanu, D., 2005, "The Impact of Shale Barriers and Injection Strategy on $CO_2$-Flooding and Sequestration Performance," paper SPE 95468 presented at the 2005 SPE Annual Technical Conference and Exhibition, Dallas, October 9-12.

Juanes, R., Spiteri, E. J., Orr, F. M., Jr., and Blunt, M. J., 2006, "Impact of Relative Permeability Hysteresis on Geological CO2 Storage," *Water Resour. Res*., 42, W12418, DOI: 10.1029/2005WR004806

Kumar, A., Noh, M., Pope, G. A., Sepehrnoori, K., Bryant, S., and Lake, L.W., 2005, "Reservoir Simulation of CO2 Storage in Deep Saline Aquifers," *SPE J.*, 10(3), 336 – 348.

Land, C. S., 1968, "Calculation of Imbibition Relative Permeability for Two and Three-Phase Flow from Rock Properties," *SPE J.*, 8(2), 149-156. Petrol. Trans. AIME, 243.

Lenormand, R., Zarcone, C., and Sarr, A., 1983, "Mechanisms of the Displacement of One Fluid by Another in a Network of Capillary Ducts," *J. Fluid Mechanics*, 135, 123-132.

Mo, S., and Akervoll, I., 2005, "Modeling Long-Term CO2 Storage in Aquifer with a Black-Oil Reservoir Simulator," paper SPE 93951 presented at SPE/EPA/DOE Exploration and Production Environmental Conference, Galveston, March 7–9.

Nghiem, L. X., Sammon, P., Grabenstetter, J., and Ohkuma, H., 2004, "Modeling $CO_2$ Storage in Aquifers with a Fully-Coupled Geochemical EOS Compositional Simulator," paper SPE 89474 presented at the SPE/DOE Symposium on Improved Oil Recovery, Tulsa, April 17-21.

Oak, M. J., Baker, L. E., and Thomas, D. C., 1990, "Three–Phase Relative Permeability of Berea Sandstone," *JPT*, 1054–1061, Trans., AIME, 289.

Press, W. H., Teukolsky, S. A., Vetterling, W. T., and Flannery, B. P., 2002, Numerical Recipes in C++: *The Art of Scientific Computing*, Cambridge University Press, Cambridge, UK, second edition.

Pruess, K., 2004, "Numerical Simulation of $CO_2$ Leakage from a Geologic Disposal Reservoir, Including Transitions from Super- to Subcritical Conditions, and Boiling of Liquid $CO_2$," *SPE J.*, 9, 237-248.

Pruess, K., Xu, T., Apps, J., and Garcia, J., 2001, "Numerical Modeling of Aquifer Disposal of $CO_2$," paper SPE 66537 presented at the SPE/EPA/DOE Exploration and Production Environmental Conference, San Antonio, February 26-28.

Remy, N., 2004, Geostatistical Earth Modeling Software: User's Manual. http://sgems.sourceforge.net/.

Sarma, P., Durlofsky, L. J., Aziz, K., and Chen, W.H., 2006, "Efficient Real-Time Reservoir Management Using Adjoint-Based Optimal Control and Model Updating," *Computational Geosciences* (2006), 10, 3-36, DOI: 10.1007/s10596-005-9009-z.

Spiteri, E. J., Juanes, R., Blunt, M. J., and Orr, F. M., 2005, "Relative Permeability Hysteresis: Trapping Models and Application to Geological $CO_2$ Sequestration," paper SPE 96448 presented at the SPE Annual Technical Conference and Exhibition, Dallas, October 9-12.

Valvatne P. H., and Blunt, M. J., 2004, "Predictive Pore-Scale Modeling of Two-Phase Flow in Mixed Wet Media," *Water Resour. Res*., 40, W07, 406, DOI: 10.1029/2003WR002, 627.

Van Genuchten, M. Th., 1980, "A Closed–Form Equation for Predicting the Hydraulic Conductivity of Unsaturated Soils," *Soil Sci. Soc. Am. J.*, 44, 892–898.

Yeten, B., Durlofsky, L. J., and Aziz, K., 2002, "Optimization of Smart Well Control," paper SPE 79031 presented at the SPE International Thermal Operations and Heavy Oil Symposium and International Horizontal Well Technology Conference, Calgary, Canada, November 4-7.

Yeten, B., 2003, "Optimum Deployment of Nonconventional Wells," Ph.D. dissertation, Department of Petroleum Engineering, Stanford University, California.